Fakultät für Medizin
Institut für diagnostische und interventionelle Radiologie
des Klinikums rechts der Isar

Multispectral Optoacoustic Tomography for Rheumatoid Arthritis

Claudio Emanuel Franz Carl Maria Freiherr von Schacky auf Schönfeld

Vollständiger Abdruck der von der Fakultät für Medizin der Technischen Universität München zur Erlangung des akademischen Grades eines Doktors der medizinischen Wissenschaft genehmigten Dissertation.

Vorsitzende(r): Prof. Dr. Jürgen Ruland
Prüfer der Dissertation:
1. Priv.-Doz. Dr. Reinhard Meier
2. Prof. Dr. Vasilis Ntziachristos

Die Dissertation wurde am 19.11. 2018 bei der Technischen Universität München eingereicht und durch die Fakultät für Medizin am 17.04.2019 angenommen.

Table of content

List of Abbreviations:

ACPA	Anti-Citrullinated Protein Antibodies
ACR	American College of Rheumatology
AuNR	Gold Nanorods
CAIA	Collagen Antibody–Induced Arthritis
CMC	Carpometacarpal
CR	Conventional Radiography
CRP	C-reactive Protein
CTAB	Cetyltrimethylammonium Bromide
DAPI	4′,6-Diamidin-2-Phenylindol
DMARD	Disease Modifying Anti-Rheumatic Drugs
dPGS	Dendritic Polyanionic Dendritic Polyglycerol Sulfate
ESR	Erythrocyte Sedimentation Rate
EULAR	European League Against Rheumatism
GC	Glucocorticoids
ICC	Indocarbocyanine Conjugate
ICG	Indocyanine Green
IL-2	Interleukin 2
MCP	Metacarpophalangeal
MSOT	Multispectral Optoacoustic Imaging
MTP	Metatarsophalangeal
MTX	Methotrexate
Nd:YAG	Neodymium-Doped Yttrium Aluminum Garnet
NIR	Near-infrared Dye
NSAID	Non-Steroidal Anti-Inflammatory Drugs
OD	Optical Density
OI	Optical Imaging
OMERACT	Outcome Measures in Rheumatology Clinical Trials
PBS	Phosphate Buffered Saline
PD	Proton Densitiy
PDUS	Power-Doppler Ultrasonography
PEG	Polyethylene Glycol
PET	Positron Emission Tomography, See
PIP	Proximal Interphalangeal
RA	Rheumatoid Arthritis
RAMRIS	RA-MRI-Scoring-System
ROI	Region of Interest
SPECT	Single-photon Emission Computed Tomography
SPIR	Spectral Presaturation with Inversion Recovery
TA	Thioctic Acid
TNF-α	Tumor Necrosis Factor Alpha
ULN	Upper Limit of Normal
US	Ultrasonography

1. Introduction

Rheumatoid arthritis (RA) is one of the most common chronic inflammatory diseases affecting around 1% of the population. RA primarily manifests in joints and is characterized by inflammation of the synovia, causing pain and stiffness in affected joints and ultimately leading to destruction of the joint. RA constitutes a major socioeconomic challenge because it causes more disability than any other chronic inflammatory disease in developed nations (Jordan et al., 2007). Therefore, extensive research is conducted to improve the outcome of the disease. The development of new therapeutic strategies has already significantly limited the progression of the disease and greatly improved the quality of life for many patients. Hereby, early diagnosis and treatment are essential for an optimal clinical outcome. Accurate and early diagnosis relies on patient history, clinical examination, laboratory testing, and imaging (Singh et al., 2016). Imaging in particular plays an increasingly important role in the diagnostic routine of patients with suspected or established RA. However, currently used clinical imaging modalities either show limitations in their diagnostic accuracy or are simply too costly for widespread application. While conventional radiography CR can readily identify severe damages to bone, its assessment of soft tissue is very limited. Ultrasonography (US) shows changes to soft tissue, however entails high inter-user variability. Magnetic resonance imaging (MRI) allows the most accurate visualization of pathological alterations to both bone, and soft tissue. It shows the highest sensitivity for the detection of synovitis, one of the earliest signs for RA. However, the maintenance and operating costs of MRI are very high, thus strongly restricting its clinical use (Zeman & Scott, 2012).

Optical imaging (OI) systems represent an interesting approach to overcome these limitations. Previous studies have shown their potential as an inexpensive and easy-to-use imaging modality with high soft tissue contrast well suited for the detection of arthritis. Most clinically applicable OI systems rely on fluorescent contrast agents to improve tissue contrast and have previously been used to detect synovitis in patients with RA (Golovko, Meier, Rummeny, & Daldrup-Link, 2011; Meier et al., 2012). However, one key limitation lies in the low tissue penetration depth of fluorescence based optical imaging. An interesting and rather recently developed imaging system with a significantly higher penetration depth is multispectral optoacoustic (MSOT) imaging. It relies on the optoacoustic effect, which is based on the emission of ultrasound waves through thermal expansion following the illumination of the specimen with light pulses. As scattering of ultrasound waves is much lower than optical scattering, optoacoustic imaging allows for deeper tissue imaging. MSOT imaging allows for tomographic high-resolution imaging with 3-dimensional reconstruction capabilities. In addition, it can easily identify different photo absorbers such as hemoglobin through multispectral imaging data acquisition at different illumination wavelengths (Ntziachristos & Razansky, 2010). A variety of photo absorbers can serve as contrast agents for MSOT

imaging, such as the clinically approved fluorescent indocyanine green (ICG). While most clinically used contrast agents rely on pathologically increased vascular permeability, more recently, there have been efforts to implement specific molecular targeting mechanisms that provide a direct visualization of an underlying molecular process such as the expression of inflammatory proteins. An interesting approach are dendritic polyanionic dendritic polyglycerol sulfate (dPGS) based contrast agents. dPGS directly bind to L- and P-selectins which are specific surface proteins that are highly expressed in inflamed tissue. Therefore, dPGS connected to a near-infrared dye (dPGS-NIR) represents a promising targeted photoacoustic contrast agent to visualize the extent of arthritic inflammation and use the imaging data to grade the degree of the inflammation. Furthermore, gold nanorods can also serve as photo absorbers, and thus can be used as contrast agents for MSOT (Mallidi et al., 2009). Gold nanorods consist of spherical golden nanoparticles that are aligned like rods with a size ranging from around 1-100nm. By coating gold nanorods with dPGS, gold nanorods could also serve as a novel inflammation targeting optoacoustic contrast agent to accurately visualize arthritic inflammation in vivo. While detection and grading of arthritic inflammation play an essential role, it is also crucial to monitor the efficacy of an appropriate therapy. Therefore, MSOT in combination with an inflammation targeting contrast agent might reveal early and decisive signs for the effectiveness and responsiveness of the therapy. This might allow for a prompt adaption of the therapy in case imaging shows a reduced therapeutic effect, and thus could improve the outcome of the disease.

1.1. Motivation and Aim

The motivation of this study was to investigate the potential of MSOT for the visualization of arthritic inflammation, and possibly provide the biomedical imaging community with an inexpensive, easy-to-use, user-independent, and accurate imaging system for the assessment of RA. In particular, the aim of this study was to evaluate MSOT for the detection and evaluation of RA in a murine model using an inflammation-targeting contrast agent. Therefore, a fully organic dPGS-NIR fluorescent photo absorber was used as a photoacoustic contrast agent. In addition, we wanted to investigate whether golden nanorods coated with dPGS are also a viable inflammation-targeting photoacoustic contrast agent for the detection of RA. To understand the meaning of the MSOT imaging findings, the imaging results were compared to MRI, clinical observation, histopathology, and blood tests. Furthermore, the aim was to develop an image analysis protocol that was easy-to-use and user-independent, and that might allow for accurate differentiation between healthy and affected joints, as well as grade the degree of arthritic inflammation. Finally, another goal was to evaluate the effect of appropriate therapy on the MSOT imaging results, in an effort to understand whether MSOT might be suitable for monitoring of treatment efficacy.

2. Theoretical background

2.1. Rheumatoid Arthritis

Rheumatoid arthritis (RA) is a chronic autoimmune inflammatory disease that mainly affects joints. The disease is characterized by chronic inflammation of the synovia leading to swollen and warm joints. This results in pain and stiffness of the joint, and ultimately leading to destruction of cartilage and bone. Additionally, the disease causes a systemic inflammation and the production of autoantibodies such as rheumatoid factor and citrullinated peptide (Smolen, Aletaha, & McInnes, 2016). Effective treatment consists of a multidisciplinary approach that contains pharmacological medication as well as physiotherapy. Medication aims to control the symptoms and decrease the progression of the disease (Singh et al., 2016). Early diagnosis through clinical examination, laboratory tests, and imaging can significantly improve outcome and progression of the disease (Finckh, Liang, van Herckenrode, & de Pablo, 2006). Overall, RA is one the most common health problems in developed nations affecting ~1% of the population and causing more disability than any other chronic disease (Jordan et al., 2007).

2.2. Pathophysiology

RA revolves around a complex pathophysiology in which overproduction of TNF plays a major role for the inflammatory response. TNF causes the activation of lymphocytes, macrophages, and synovial fibroblasts (Feldmann, Brennan, & Maini, 1996). Macrophage-like synoviocytes are the main driver for a chronic inflammation through the overexpression of a range of cytokines (Gaffen, 2009), while fibroblast-like synoviocytes invade the cartilage and activate osteoclasts causing bone destruction (Muller-Ladner et al., 1996).

Furthermore, the production of autoantibodies plays an important role in the development of the disease. One of the two long-established autoantibodies is rheumatoid factor, an antibody against the Fc portion of IgG antibodies. The other being anti-citrullinated protein antibodies (ACPA), an antibody against citrullinated proteins (Puszczewicz & Iwaszkiewicz, 2011). These antibodies are present in around 80% of RA patients and help diagnose the disease. High concentrations of these antibodies increase the probability of RA. However, they are not specific for RA and can also be present in chronic infections like hepatitis C and chronic inflammatory diseases like systemic lupus (Farheen & Agarwal, 2011). Moreover, differences can be found between patients in which both antibodies are present to the so-called autoantibody-negative RA patients. Antibody-positive patients have more severe joint damage and lower remission rates (van der Helm-van Mil, Verpoort, Breedveld, Toes, & Huizinga, 2005).

As the disease progresses, the proliferation of fibroblast-like synoviocytes at the border of the joint causes the formation of granulation tissue called pannus. In the course of this formation

and under the influence of macrophages and lymphocytes, autolytic enzymes are released. This leads to the destruction of bone and cartilage, as well as the expansion of the pannus. In final stages of RA, complete dislocation and ankylosis of the destroyed joints can be observed (Furuzawa-Carballeda, Macip-Rodriguez, & Cabral, 2008).

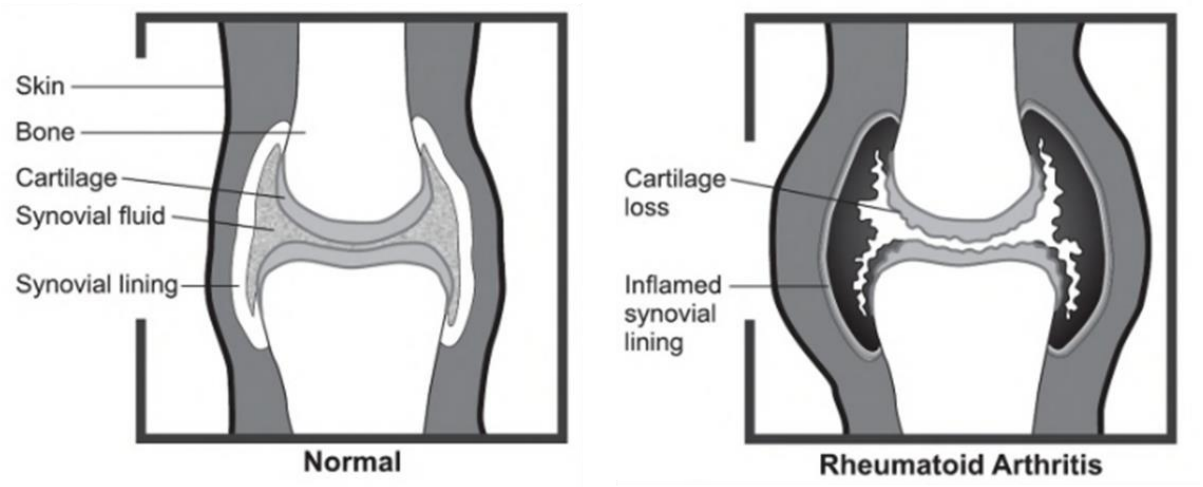

Figure 1: While a normal healthy joint does not show any pathological alterations, RA leads to an enlargement of the synovia in the affected joint. Hereby, fibroblast-like synoviocytes, invade and proliferate in the joint in a chronic inflammation driven by a macrophage-like synoviocytes. This ultimately leads to destruction of the bone and cartilage through activation of osteoclasts (Cush, 2010).

2.3. Diagnosis

Diagnosis of RA relies on patient history, clinical examination, laboratory testing, and imaging. In 2010, the American College for Rheumatism (ACR) and the European-League-Against-Rheumatism (EULAR) updated their standardized clinical criteria Rheumatoid-Arthritis-Classification-Criteria (RACC) for the diagnosis of RA. The former criteria from 1997 had low sensitivity at early stages of RA and were usually met when the joints had already suffered irreversible damage. Additionally, the criteria did not take anti-citrullinated protein antibodies (ACPA) into account. The current criteria are focused on the detection of earlier stages of RA to allow for an early treatment. This helps reduce the progression of the disease and the manifestation of symptoms (Aletaha et al., 2010). The criteria contain the evaluation of joint involvement, duration of symptoms, and blood tests for inflammatory parameter and specific antibodies.

A joint is considered involved with clinical signs of synovitis if it is swollen or tender on examination. Some patients with inflamed joints show signs for a systemic inflammation like acute phase reactants, autoantibodies, and morning stiffness of the joints. These patients have a higher likelihood of developing or having RA (van der Helm-van Mil et al., 2008).

C-reactive protein (CRP) and erythrocyte sedimentation rate (ESR) are two typical acute phase reactants, that often times show abnormal values in a state of systemic inflammation. CRP is an acute phase protein and its production in the liver is mainly induced through Interleukin 6 (IL-6) beside other inflammatory impulses. Elevated CRP levels are an unspecific sign for an acute inflammation of both infectious and non-infectious origin. In patients with chronically inflamed joints, it can be a sign for RA. ESR is one of the oldest laboratory tests to determine a state of unspecific systemic inflammation. Hereby, elevated blood concentration of acute phase proteins cause an agglomeration of erythrocytes and thus a prolonged sedimentation time. ESR takes at least 24h to surpass a discernable threshold, while CRP values rise after 2 hours. Both parameters are a sign for RA, and are a part of the ACR/EULAR diagnostic criteria. The criteria also differentiate small from large joints. Inflammation of multiple small joints constitute a clear sign for RA, while inflammation of large joints is not as typical. “Small joints include “metacarpophalangeal (MCP), proximal interphalangeal (PIP), second through fifth metatarsophalangeal (MTP), and thumb interphalangeal (IP) joints, and the wrists. They do not include carpometacarpal (CMC), first metatarsophalangeal (MTP) joint, or distal interphalangeal (DIP) joints, which are often affected by osteoarthritis. shoulders, elbows, hips, knees, and ankles. “

Moreover, ACPA and RF levels are graded into negative, low- and high-positive. Negative is considered less than or equal to the upper limit of normal (ULN), while positive means higher than ULN. Positive is differentiated into low-positive (≤3 x ULN) and high-positive (>3 x ULN). CRP and ESR abnormal levels are defined by the local laboratory standards.

Table 1: Criteria ACR/EULAR RACC (Aletaha et al., 2010):

Target population: patients who have at least 1 joint with clinical synovitis/swelling and it is not better explained by another disease		Score
A: Joint involvement	1 large joint	1
	2-10 large joints	2
	1-3 small joints (with/without involvement of large joints)	3
	4-10 small joints (with/without involvement of large joints)	4
	> 10 joints (at least 1 small joint)	5
B: Serology	Negative RF and negative ACPA	0
	Low-positive RF or low-positive ACPA	2
	High-positive RF or high-positive ACPA	3
C: Acute-phase reactants	Normal CRP and normal ESR	0
	Abnormal CRP or abnormal ESR	1
D: Duration of symptoms	< 6 weeks	0
	>=6 weeks	1

If the score is above or equal 6, RA can be diagnosed. A score beyond 9 signifies a severe form of RA. This means for example, that the disease can be diagnosed solely through joint inflammation in 4 MCP joints with a duration of more than 6 weeks. Additionally, it is useful to evaluate the score over time to monitor activity and progression of the disease, as well as efficacy of the therapy. (Aletaha et al., 2010)

2.4. Treatment

Treatment of RA aims to control the symptoms and decrease the progression of the disease. The treatment of symptoms relies on analgesics and non-steroidal anti-inflammatory drugs (NSAID) to reduce pain, swelling, and stiffness of the joint (Singh et al., 2016). Disease modifying anti-rheumatic drugs (DMARD) such as Methotrexate are an essential part of medication and can substantially decelerate the progression of the disease (Buer, 2015; Dekkers, Schoones, Huizinga, Toes, & van der Helm-van Mil, 2017). More recently biologicals, a class of antibody based pharmaceuticals, have gained importance in the drug therapy of RA (Singh et al., 2009). DMARD can reduce joint damage and also improve symptoms of the disease. Finally, supportive treatment with physiotherapy represent an integral part of the treatment approach. The ultimate therapeutic goal is remission, as RA cannot be cured (Singh et al., 2016).

DMARD are a group of RA medication that contain cytostatic drugs (methotrexate, azathioprine, cyclophosphamide), and other immunosuppressant drugs (leflunomide, sulfasalazine, hydroxychloroquine, ciclosporine) beside biologicals. Methotrexate inhibits dihydrofolate reductase and is the central part of the therapeutic regiment in RA. Biologicals are essentially antibodies against different parts of the immune response. Most importantly, they attack TNF-α (etanercept, infliximab, adalimumab), IL-2 (anakinra), and IL-6 (tocilizumab) (Buer, 2015). Out of DMARDs, Methotrexate (MTX) is typically the first and most important medication for patients with RA. It is combined with folic acid to decrease possible side effects. Prime alternatives for MTX in case of intolerance are sulfasalazine and leflunomide. DMARD achieve their effect through inhibition of the abnormal autoimmune response in patients with RA. Overall, DMARD reduce swelling, and stiffness of the joint, and decrease damage to the joint very effectively. DMARD can also cause serious adverse effects such as immunosuppression, liver and lung damage (Donahue et al., 2008).

Historically, glucocorticoids (GC) have played an essential role in the therapy of RA. GC reduce synovitis and decrease damage to the joint such as bone erosions, bone edema, and cartilage thinning. Subsequently, GC can significantly improve the symptoms of the disease. However, the use of GC, especially the long-term use, can cause a wide range of serious adverse effects: immunodeficiency, osteoporosis, hyperglycemia, electrolyte imbalances, beside many more. Thus, the use of GC has been discussed controversially (Ravindran, Rachapalli, & Choy, 2009).

NSAID can significantly improve the symptoms of the disease, but do not improve the prognosis of the patient while causing considerable adverse effects such as gastro-intestinal bleeding, cardiovascular problems, and renal insufficiency. Thus, the application of NSAID is controversial, and the dose and duration of NSAID treatment should be as limited as possible. Overall, NSAID can be used to treat acute flares, but long-term use is problematic (Chen et al., 2008; Wienecke & Gotzsche, 2004).

The American College of Rheumatology (ACR) developed new treatment recommendations for the treatment of rheumatoid arthritis in 2015 as an update to their previous 2012 guidelines (Singh et al., 2016): The guidelines revolve around a treat-to-target treatment approach. This includes aiming for remission or low disease activity as treatment goals, monitoring the treatment outcome, and adapting the therapy accordingly. Treatment monitoring consists of evaluation of clinical signs, and assessment of imaging findings over time. Treatment evaluation should take place every 6 to 12 weeks. The guidelines differentiate between early RA (symptoms <6 months) and established RA (≥6 months). For early RA, the aim is to minimize disease activity, possibly achieve remission, and prevent any potential lasting damage to joints. For established RA, the goal revolves around preventing any further damage, and reducing the activity to a disease, ultimately also aiming for remission. Generally, a

DMARD monotherapy with methotrexate (MTX) is preferred, though therapy should be modified under certain circumstances. As the guidelines are very complex and partly contain low evidence levels for some cases, only the main parts of the guidelines are mentioned here: Patients with both early and established RA should initially take DMARD monotherapy, preferably with MTX. If the disease activity remains moderate to high under DMARD monotherapy, treatment should consist of either a combination of DMARDs or a TNF or non-TNF biological. In patients with established RA and high activity levels under DMARD monotherapy, the treatment can be changed to a biological therapy with MTX. Under continuous high activity levels despite TNF-therapy, TNF treatment can be combined with one or two DMARD. Additionally, glucocorticoids (GC) can be used in acute flares, or to extend the therapy for moderate to high disease activity levels. However, GC should be restricted to the lowest possible dose for the lowest possible duration, to minimize possible side effects.

2.5. Imaging

Imaging plays an important role in the diagnostic approach of RA. It can be used to assess bone erosions, joint space narrowing, synovitis, and soft tissue swelling. Based on the ACR/EULAR criteria, RA can be diagnosed if two typical bone erosions are visible through imaging. Additionally, imaging can be used to determine changes of the joint to monitor the development of the disease and evaluate the effect of the therapy.

Conventional radiography (CR) is still the most commonly used imaging modality even though it can only detect changes in the later stages of arthritis, when bone and cartilage have already been severely damaged. CR can show bone erosions, joint space narrowing, and severe swelling of the soft tissue. However, as the diagnostic focus has shifted towards earlier detection of RA other imaging modalities become more important. Mainly, magnetic resonance imaging (MRI) and ultrasonography (US) have developed into important imaging techniques to detect early changes of the joint in RA. Using contrast agent enhanced MRI, synovitis can be readily detected and evaluated. High resolution ultrasonography can reliably show bone erosions and changes in the morphology of the joint like thickening of the synovia. Ultrasonography color doppler can additionally assess synovial inflammation through changes in the vascular activity. CT is rarely used, as it is inferior to MRI, and exposes the patients to considerable amounts of ionizing radiation (Sommer et al., 2005). However, when exact visualization of bone structures for preoperative planning or exact assessment of bone damage is needed, CT imaging might be required. Molecular imaging using PET, SPECT, or other new imaging techniques like optical imaging play an increasingly important role in the evaluation of arthritic inflammation (Zeman & Scott, 2012).

2.5.1. Conventional Radiography (CR)

CR is cheap, fast, readily available, and can easily detect more severe damages such as erosion and destruction of the bone, joint space narrowing, and extensive soft tissue swelling. It relies on ionizing planar x-ray imaging. Even though CR findings do not constitute a part of the scoring system for ACR/EULAR criteria anymore after they were renewed in 2010, it is still routinely used to evaluate the stage and the progression of the disease and used a prognostic factor (Ostergaard, Ejbjerg, & Szkudlarek, 2005). CR scoring systems such as the Larsen's or Sharp's method are very reliable and have low user dependent variance (Cuchacovich, Couret, Peray, Gatica, & Sany, 1992).

In early stages, indirect signs for arthritis such as expansion of the joint space, and increased radiolucency of the bone caused by edema or reduction of bone mass can be found using CR. However, these signs are unreliable and difficult to diagnose (Bugatti, Manzo, Caporali, & Montecucco, 2012).

Direct signs for arthritis visible through CR involve destruction of bone and cartilage, and are usually developed at later and more severe stages of the disease. The destruction of cartilage causes the surrounding bone to be in direct vicinity of the joint space. This subsequently leads to the aspect of a narrowed joint space, as the space with higher radiolucency has decreased. Bone lesions are well-defined discontinuities of the cortex and visible in CR in two plains, and bone erosions represent the loss of bone in a specific area. During the course of the disease, the areas with bone and cartilage destruction expand, causing subluxation and deviation of the affected joints (Ideguchi, Ohno, Hattori, Senuma, & Ishigatsubo, 2006).

However, CR has specific limitations. CR has low soft tissue contrast, and thus detection of changes to soft tissue such as synovitis is very limited. As typical early signs for RA are alterations to synovia and soft tissue, it is very difficult to diagnose RA early through CR. Additionally, CR projects the 3-dimensional structure of the joint onto a single planar image. This constitutes a loss of anatomical information compared to tomographic imaging modalities such as MRI and CT. A study showed that MRI can detect bone erosions in ~3 times as many patients as CR with RA at 4 months after symptom onset (McQueen et al., 1998).

2.5.2. Magnetic Resonance Imaging (MRI)

MR imaging is a non-ionizing, non-invasive imaging technique based on nuclear magnetic resonance. It acquires imaging data from radio frequency signals emitted by atomic nuclei after they have been exposed to specific radio pulses in an external magnetic field. Using reconstruction algorithms, a tomographic image is calculated and allows for 3-dimensional reconstruction (McRobbie, Moore, Graves, & Prince, 2017). It offers high anatomical resolution and high soft tissue contrast. Furthermore, contrast agents can increase tissue contrast e.g. through intravenous injection of the contrast agent. Most contrast agents are solutions of

organic gadolinium complexes, a paramagnetic compound that can accumulate in abnormal tissue (Raymond & Pierre, 2005).

Overall, this results in favorable qualities for the detection and evaluation of RA as it can easily assess alterations to the synovia, cartilage, and bone. The use of contrast agent allows for the evaluation of contrast agents dynamics and enhancement of tissue. As gadolinium based contrast agents accumulate in inflamed tissue, inflammation of the joint, and more specifically inflammation of the synovia lead to high contrast agent enhancement in these areas. Additionally, MR can easily reveal alterations in the bone such as edema and erosions, as well as thinning and other changes of the cartilage. Especially for the detection and evaluation of bone erosions, MR offers the highest sensitivity from all readily available imaging modalities, facilitating the staging of the severity of bone erosions (McQueen, 2014). That's why it is considered the best imaging modality for imaging of RA (Sommer et al., 2005).

Even though MR imaging has evolved into the gold standard for imaging of RA, it has some limitations to its use. It is the most expensive widely used imaging modality, and is not as readily available as conventional radiography or ultrasonography. Acquisition times are rather long, and confined use for particular joints is necessary (McQueen, 2014). If a patient moves during image acquisition, this results in movement artifacts and can severely impair image quality. Also, patients with magnetic objects in their bodies such as pacemakers and cochlear implants may be banned from MRI, as magnetic compounds can move, be damaged, or heat up during the imaging procedure (McRobbie et al., 2017).

All in all, MRI has developed into one of the most reliable imaging modalities for RA, as it can detect and evaluate different pathologic alterations with a very high sensitivity. Additionally, the imaging results are relatively easy to reproduce and have a relatively high inter-reader agreement allowing for a standardized staging and grading of RA (Ostergaard et al., 2001).

RAMRIS (RA-MRI-Scoring-System) is the most commonly used MR imaging grading and staging method for RA, and has been developed by the OMERACT-committee (Outcome Measures in Rheumatology Clinical Trials) in 2002 (Ostergaard et al., 2003). Hereby, MCP joints II-V and the hand-wrist are evaluated regarding the severity of synovitis, bone edema, and bone erosions of in a standardized manner. Images are acquired with a T2 weighted fat saturated sequence, and in two planes with a T1 weighted sequence before and after the intravenous injection of a gadolinium based contrast agent. Synovitis is defined as an enlarged synovial compartment that shows above normal enhancement after contrast agent application. Bone erosions are defined as "sharply marginated bone lesion, with correct juxta-articular localization and typical signal characteristics." Finally, a bone edema is a lesion in the trabecular bone that shows increased water content and does not have well-defined borders. These lesions are then graded from 0-3, with 0 being normal, and 1-3 being mild, moderate and severe pathologies, respectively (Østergaard et al., 2005). The scoring system has very

high intra- and inter-reader reliability and can detect changes with a high sensitivity (Haavardsholm et al., 2005). Furthermore, the results correlate with the clinical activity level of the disease, and with histopathological signs for synovitis (Gandjbakhch et al., 2014).

2.5.3. Ultrasonography (US)

Ultrasonography (US) is a non-ionizing diagnostic imaging technique based on the reflection and detection of ultrasound. Images are calculated from the sound echoes emitted from tissue that has previously been reached by ultrasound waves. An ultrasonography device consists of a piezoelectric transducer, that can emit short ultrasound pulses and can detect the corresponding sound echoes.

US provides real-time imaging with high soft tissue contrast at low-cost using a portable device. Using the b-mode, a mode which shows the scanned plane as a 2-dimensional image, structural changes can be easily assessed. Power-Doppler US (PDUS) relies on the doppler effect and allows for measurements of blood perfusion. As US relies on the transmission of ultrasound waves, imaging through air or bone corrupts the image. Furthermore, the penetration depth is limited, especially in tissue with low ultrasound transmission properties.

For RA, however, it has evolved into one of the most widely used imaging modalities. US can easily detect changes to the joint in RA, as it has high soft tissue contrast, and can additionally measure changes in the perfusion of the joint, visualizing inflammatory hyperperfusion of the joint. An enlarged synovia with increased blood flow is a clear sign for synovitis. Furthermore, US can determine bone erosions, and alterations to the cartilage such as thinning. It is especially good at evaluating tendons, and alterations to tendons such as tenosynovitis and ruptures of the tendon. It can also be used to visualize invasive punctures of joint e.g. to treat an effusion. US has low image acquisition times, and as opposed to CR does not use ionizing radiation. Compared to MRI, US is readily available and significantly cheaper. However, its main draw-backs in the imaging of RA is the difficulty of visualizing bone or structures behind bone. Moreover, it is very user-dependent, and the experience of the user plays an important role in the sensitivity of the modality (Tan, Ostergaard, & Conaghan, 2012).

2.6. Importance of early diagnosis and imaging

Early diagnosis and early effective treatment is pivotal for a favorable outcome in patients with RA. Early diagnosis and early effective treatment can substantially decrease potential symptoms, prevent damage to the joint, and increase the likelihood of remission (Finckh, 2009). However, ACR criteria alone are often times insufficient to diagnose early RA (van der Helm-van Mil & Huizinga, 2012). As synovitis is one of the first signs in the course of RA, the diagnostic importance for imaging has grown. As US and MRI can reliably detect synovitis, they can facilitate an early diagnosis and treatment, especially in cases, where the clinical

signs for RA remain inconclusive. It has been shown that the use of these imaging modalities in patients with suspected early RA can positively influence the outcome and course of their disease regarding symptoms (Hodgson, O'Connor, & Moots, 2008; M. Y. Wang, Wang, Sun, Liu, & Huang, 2016). However, MRI is not routinely performed for every patient as it is very costly (Tan et al., 2012).

2.7. Molecular Imaging methods

Classic imaging approaches using US, MRI, and CR revolve around revealing anatomical structures and morphologic alterations caused by RA. However, they do not show the underlying pathophysiological alterations in inflammatory biochemical pathways, or pathologic cellular changes (Wunder, Straub, Gay, Funk, & Muller-Ladner, 2005). Molecular imaging as a whole tries to overcome these limitations, by revealing functional changes on a molecular level. Positron emission tomography (PET) and single-photon emission computed tomography (SPECT) are two major nuclear imaging techniques that are used in clinical practice for this purpose. They rely on target-specific tracers to visualize a particular molecular structure. These imaging techniques can identify abnormal molecular alterations before anatomical changes are visible, subsequently allowing for earlier detection of RA than classic imaging approaches (Pichler, Wehrl, & Judenhofer, 2008). Additionally, molecular imaging can identify patients that are sensitive to a specific medication before the medication is applied regularly. This avoids inefficient treatment, prevents adverse drug effects, and saves costs as especially biological therapy is very expensive. After the start of regular treatment, effective and precise monitoring of treatment success based on biochemical markers is possible. However, PET and SPECT are not only very expensive and rarely available medical imaging procedures, but also expose the patients to considerable amounts of ionizing radiation (Wunder et al., 2005). Thus, recent research focuses on developing new molecular imaging techniques without ionizing radiation. A promising new imaging approach - optical imaging - is based on optical illumination of the specimen and does not cause ionizing radiation because it uses laser wavelengths in the near-infrared spectrum (Put, Westhovens, Lahoutte, & Matthys, 2014).

2.8. Optical Imaging (OI)

Optical imaging (OI) is based on the use of light for image acquisition and includes bioluminescence and fluorescence imaging. Historically, they have been mostly used for microscopic imaging, but have recently been developed for large scale imaging. OI uses light from the near-infrared spectrum, which contains visible red light and invisible infra-red light for illumination, as they belong to the non-ionizing light spectrum in contrast to light from the ultraviolet spectrum (Muller, Wunder, & Licha, 2013). In the case of bioluminescence, light is directly emitted from the specimen, and detected externally by a charge-coupled device (CCD).

Fluorescence imaging, however, relies on the detection of a specific fluorescence wavelength emitted by fluorophores following laser excitation at the excitation wavelength.

For the purpose of imaging RA, 2-dimensional optical imaging has been explored. Hereby, images are acquired through planar illumination of the hands, where light is detected after it has passed through the scanned tissue. This way, not only fluorescent signal can be measured, but also tissue absorbance characteristics. Primarily, oxy- and deoxygenated blood yield very specific light absorption properties in the red- and infra-red spectrum (Muller et al., 2013). Using reconstruction algorithms, this allows for the visualization of oxy- and deoxygenated blood as “natural contrast agents” (McQueen et al., 1998). Patients with RA typically show abnormal light absorption characteristics of the hand because the hands will typically be hyperperfused resulting in an increased amount of absorption by oxy- and deoxygenated blood. In addition, joint edema and joint effusion can also be detected because of altered light absorbance (Scheel et al., 2005). Furthermore, fluorescent contrast agents such as indocyanine green (ICG) can be used to enhance tissue contrast and visualize blood flow for the detection of RA (Meier et al., 2010). ICG is an FDA-approved carbocyanine dye that has been routinely used for ophthalmologic angiography for over 40 years. It classifies as an unspecific dye because it does not have a specific targeting mechanism and binds to 98% to plasma proteins. However, in inflamed joints the vascular hyperpermeability allows ICG to extravasate into the inflamed soft tissue (Andersson, Lexmuller, & Ekstrom, 1998). Generally, OI systems have fast image acquisition times and are inexpensive while yielding good soft tissue contrast. However, the tissue absorption of light is not only the means to produce an image, it is also the main limitation of OI overall. Light has a very limited travel distance in tissue before the illumination is too low for image acquisition. This means that tissue can only be examined up to a depth of several mm depending on the imaging technique (Adrian Taruttis & Ntziachristos, 2012).

Moreover, a first commercially available and easy-to-use optical imaging device “Xiralite X4 Rheumascan” for the detection and evaluation of arthritis has been developed by Mivenion, Berlin. This ICG-enhanced optical imaging system excites the fluorescent dye at 740nm and detects the filtered (800nm) emitted fluorescence signal with a CCD. As shown in figure 2, this OI system showed perfusion of the joint through images comparable to those of MRI for the detection of hyperperfusion and synovitis. Therefore, the accuracy of the “Xiralite X4 Rheumascan” in the detection and evaluation of arthritis was investigated in a patient study. For comparison, all 45 patients underwent both imaging with the “Xiralite X4 Rheumascan” and MR imaging at the same timepoints as MRI is considered the most accurate and reliable RA imaging modality. However, the “Xiralite X4 Rheumascan” showed limitations regarding the detection of inflamed joints compared to MRI (Meier et al., 2012).

Furthermore, a tomographic fluorescence based optical imaging system, the so called fluorescence molecular tomography (FMT), has also been used to detect synovitis in patients through the evaluation of ICG-contrast enhancement. The study relied on an OI system with a fluorescence-based image acquisition and tomographic image reconstruction capabilities. This allowed for accurate and high spatial resolution with the ability for 3-dimensional reconstruction. The FMT findings correlated with MR imaging results and inflamed joints could be distinguished from healthy joints through synovial hyperperfusion (Mohajerani et al., 2014).

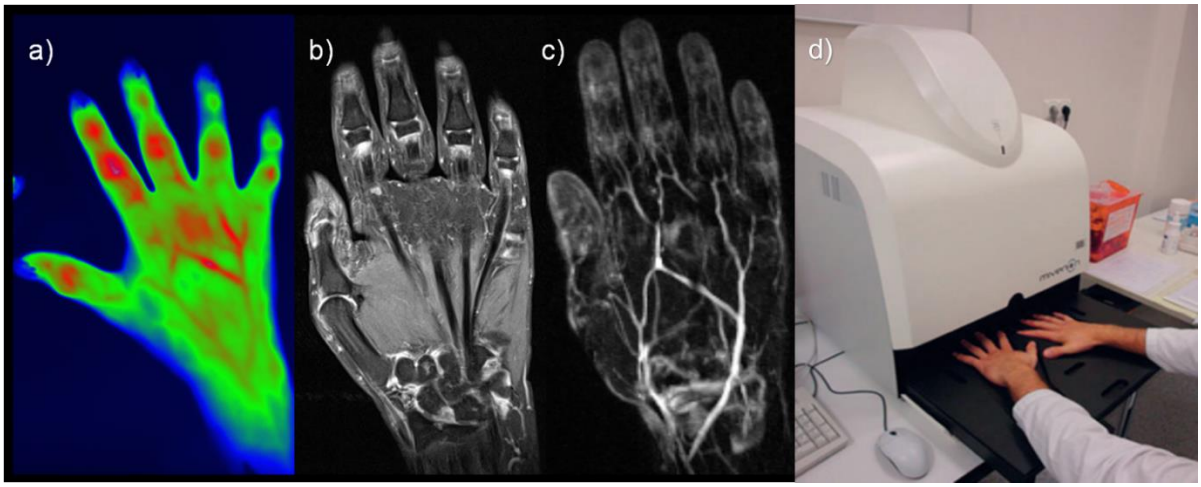

Figure 2: a) Image of the hand using the Xiralite X4 Rheumascan with focal hyperperfusion in the joints of MCP D III and IP, as well as PIP and DIP of II-V. b) c) Corresponding MR image revealing mild to moderate inflammatory signs in the same joints. d) Xiralite X4 Rheumascan imaging setup (Sievert, 2015).

2.9. Multispectral Optoacoustic Tomography (MSOT)

Multispectral optoacoustic imaging is based on the optoacoustic effect. Hereby, the specimen is illuminated with short high-power laser pulses with a certain frequency that cause warming and thermal expansion of the specimen. The periodic high-frequency thermal expansion then generates ultrasound waves that then can be recorded using ultrasound detectors which are positioned around the specimen. Based on this data an image can be reconstructed with different inversion algorithms. As scattering of ultrasound waves is substantially lower than optical scattering, optoacoustic imaging allows for deeper penetration depths and a more reliable image acquisition (Ntziachristos, 2010).

The newly developed multispectral optoacoustic tomography imaging system uses circularly aligned laser diodes to achieve even illumination at different wavelengths with a tunable laser. The emerging ultrasound signal is then recorded by circularly positioned ultrasound detectors, to allow for tomographic image reconstruction. This way an anatomical image can be obtained. Furthermore, the specimen can be illuminated at different wavelengths in the near-infrared

spectrum ranging from 680 nm - 980 nm (Ma, Taruttis, Ntziachristos, & Razansky, 2009). Using spectral unmixing, MSOT can account for different light absorbing entities that have specific absorption characteristics such as deoxy- and oxygenated hemoglobin, and fat (X. Wang, Xie, Ku, Wang, & Stoica, 2006). Additionally, appropriate optical contrast agents such as ICG can be identified based on their specific absorption spectrum. In this regard, ICG is not used for its fluorescent properties, but for its particular light absorption pattern in the near-infrared spectrum. Moreover, dyes like ICG can be equipped with a targeting mechanism to allow for molecular imaging of certain structures or biochemical pathways (Herzog et al., 2012). Overall, this allows for anatomical image acquisition and molecular imaging of underlying molecular activities simultaneously.

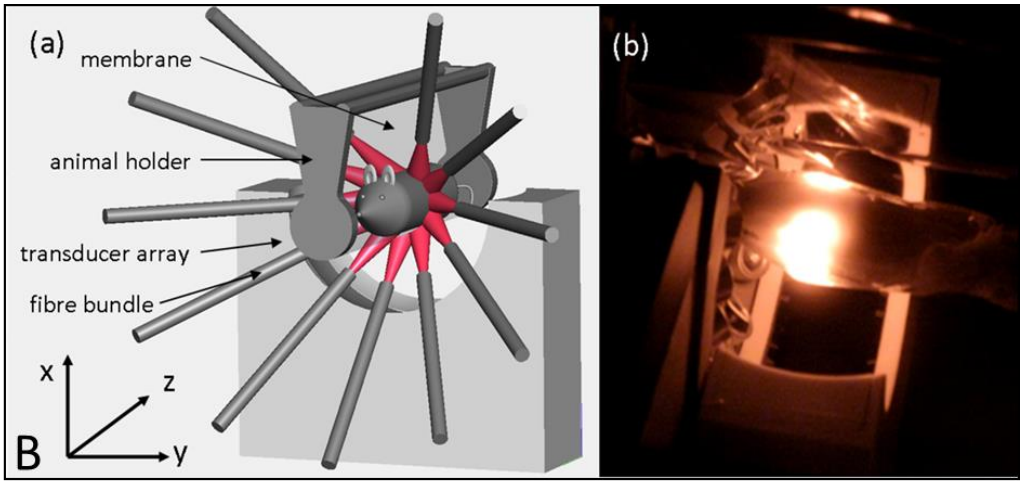

Figure 3: a) Schematic illustration of the MSOT imaging setup: the mice is fixated on a moving stage and illuminated evenly by circularly arranged laser fibre bundles. An ultrasound transducer array detects the emitted photoacoustic signal. b) Image of the MSOT imaging processes: A mouse is illuminated on the moving stage. The mouse is encased in a polyethylene layer filled with water up to the head so that it can still breath normally. The whole stage is under water to ensure optimal ultrasound propagation to the transducer array (Razansky, Buehler, & Ntziachristos, 2011).

2.10. Contrast Agents for Optical and Optoacoustic Imaging

Generally, contrast agents for MSOT should have a specific absorption spectrum in the near-infrared light spectrum that can be easily distinguished from the absorption characteristics of the “tissue background”. This way, spectral unmixing of the contrast agent signal leads to a very accurate and reliable visualization of the localization and accumulation of the contrast agent. Additionally, the contrast agent can contain a targeting mechanism, leading to accumulation at the targeted structures. In RA, components of inflammatory pathways constitute potential targets. Inflammation targeting contrast agents could easily detect arthritic

inflammation even in the absence of observable morphological alterations (Ibarra, Jimenez, Martinez, Clark, & Ahuja, 2011).

2.10.1. Polyanionic dendritic polyglycerol sulfate near-infrared dye (dPGS-NIR)

The main contrast agent in this study was a near-infrared dye (NIR) that was connected to polyanionic dendritic polyglycerol sulfate (dPGS). Previous research has studied the application of dPGS as a new medication to inhibit inflammation (Dernedde et al., 2010). dPGS binds to P- and L-selectins, which are transmural proteins that are highly expressed on the surface of inflamed tissue. L-selectin is present on the surface of leukocytes, while P-selectins are endothelial proteins. Selectins are cell adhesion molecules that play an important role in the leukocyte extravasation process (Ley, Laudanna, Cybulsky, & Nourshargh, 2007). dPGS has a similar molecular structure as natural ligands and binds to L- and P-selectins very efficiently. In a murine model, application of dPGS showed to inhibit leukocyte extravasation and inflammatory effects such as edema (Dernedde et al., 2010).

However, dPGS can also be used to synthetize an optical contrast agent with very efficient inflammation targeting properties. A dPGS conjugate with a near-infrared dye (NIR) similar to ICG was used to visualize inflamed tissue with an in vivo fluorescence imaging system in a RA rat model. The dPGS-NIR probe accumulated strongly in the inflamed joints, allowing for differentiation of affected and healthy joints. The accumulation of dPGS-NIR was additionally confirmed histopathologically. In contrast, the NIR dye without an inflammation targeting mechanism did not accumulate in inflamed joints (Licha et al., 2011). In further studies, dPGS-NIR was shown to reliably and accurately visualize inflamed tissue through in vivo fluorescence imaging in an asthma murine model (Biffi et al., 2013). However, these studies relied on planar 2-dimensional imaging, thus not allowing for the calculation of tomographic images, or 3-dimensional reconstruction, thus limiting accurate spatial assessment of the imaged structures. Moreover, studies have investigated the potential of dPGS-NIR for MSOT imaging of myocardial infarction. In a murine model, MSOT could detect infarcted myocardium and differentiate it from healthy tissue based on the accumulation of dPGS in the injured areas. Through histopathological analysis, these findings could be confirmed with leukocytes and endothelium as main sources of the dPGS signal. MSOT offered high anatomical resolution of less than <200µm and allowed for 3-dimensional reconstruction to accurately evaluate the extend of the myocardial infarction (A. Taruttis et al., 2013).

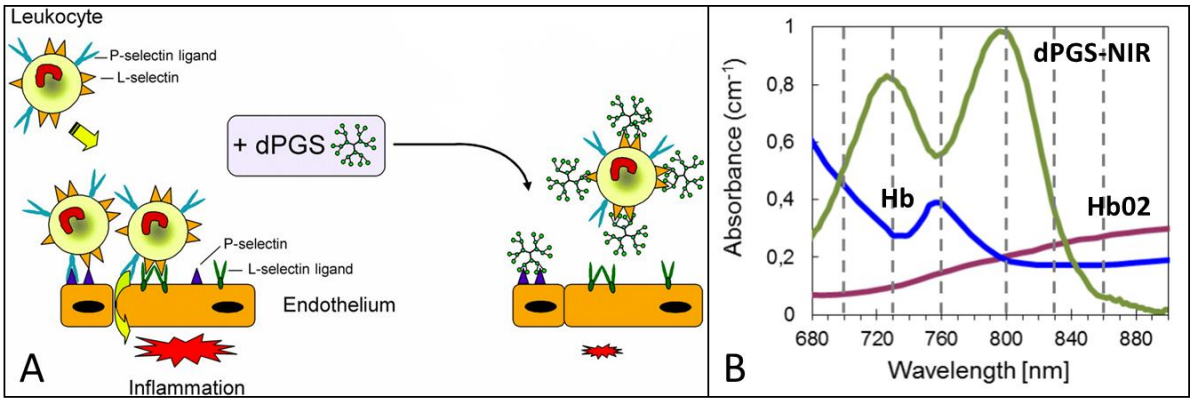

Figure 4: A: Schematic illustration of the dPGS targeting mechanism: dPGS bind to L- and P-selectins - transmural surface proteins that are expressed on the endothelium and on leukocytes during inflammation and help leukocyte extravasate into the tissue. Thus, dPGS also inhibits inflammation through blocking these selectins (Dernedde et al., 2010). B: Light absorption spectra of dPGS-NIR, oxygenated (Hb02) and deoxygenated (Hb) hemoglobin. MSOT can easily differentiate those through evaluation of the photoacoustic signal at different illumination wavelengths in the near-infrared light spectrum (680nm-900nm) (Dernedde et al., 2010).

2.10.2. Gold Nanorods (AuNR)

Gold nanorods (AuNR) contain spherical nanoparticles with a diameter of ~4nm that have been aligned like rods through a specific synthesis. The size of nanorods can range from around 1-100nm in each dimension depending on the application. After the initial synthesis process, the nanorods are typically covered by a cetyltrimethylammonium bromide (CTAB) layer. CTAB is cytotoxic, which is why the CTAB layer is usually replaced by a biocompatible layer such as polyethylene glycol (PEG). In further synthesis steps, the AuNR coat can be modified to offer the biochemical properties as desired (Murphy et al., 2005). AuNR absorb light along the short and the long axis, resulting in two absorption bands. An increase in the rod length leads to a red shift of the absorption band, thus allowing for customized absorption characteristics well adapted for near-infrared optical imaging (Stone, Jackson, & Wright, 2011). In addition, AuNR can change their morphology and subsequently their absorption properties depending on their local environment, facilitating the use as sensors for their biological environment (Yu & Irudayaraj, 2007). Furthermore, the morphology of AuNR changes when exposed to specific laser light pulses, thus enabling the use of AuNR as vehicles for drug delivery (Guerrero et al., 2014).

AuNR with an appropriate targeting mechanism have been used as targeted contrast agents for optoacoustic imaging. AuNR have been used to detect cancer through conjugation with an antibody against epidermal growth factor (Mallidi et al., 2009). Furthermore, AuNR has also been used to visualize inflammation, and more specifically RA. AuNR targeting matrix metalloproteinase-2 – a protein responsible for degradation of extracellular matrix and part of

the inflammatory response - have been used to evaluate atherosclerotic plaques (Qin et al., 2016). Moreover, AuNR has also been used to visualize RA through a TNF-α targeting antibody in a murine model of arthritis. The aforementioned studies however, all used a planar optoacoustic imaging system with a single focused ultrasound transducer, thus not allowing for tomographic image acquisition (Fournelle et al., 2012).

For MSOT imaging, untargeted gold nanorods have been used to determine vascular permeability and retention characteristics of tumorous tissue (Herzog et al., 2012). A targeted approach to reveal pancreatic tumors through MSOT was based on gold nanorods coated by an acidic pH-targeting mechanism. This facilitated the detection of abnormal tumorous tissue through its altered pH-microenvironment (Zeiderman et al., 2016).

AuNR, however, can also be coated with polyanionic dendritic polyglycerol sulfate (AuNR-dPGS) to also target the inflammatory glycoproteins L- and P-selectin. This should analogously result in similar accumulation characteristics as dPGS-NIR and lead to an accurate visualization of inflammation.

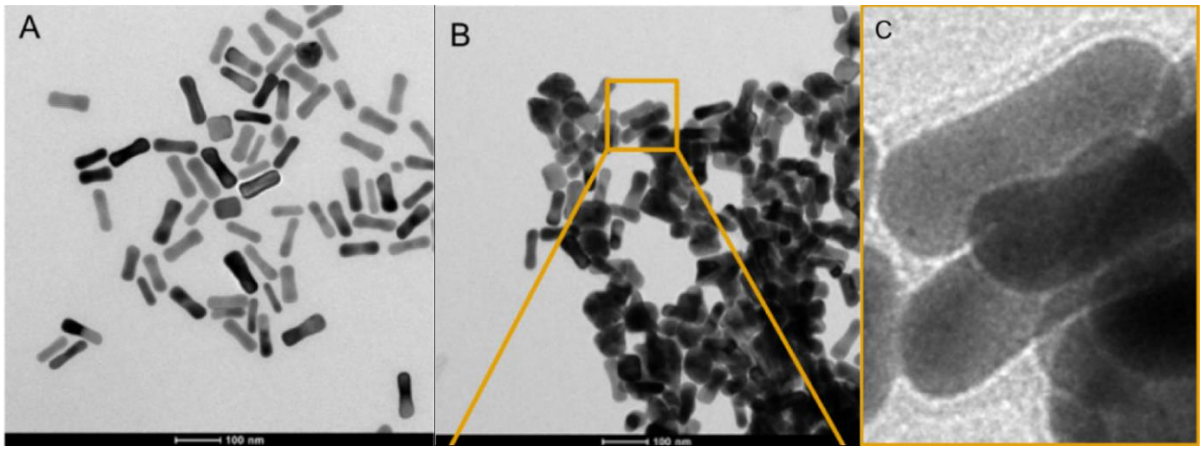

Figure 5: Transmission electron microscopy images of purified AuNR-dPGS incubated with (A) NaCl and (B) BaCl2 at an ionic strength of 100 mM. (C) Magnified image from (B) shows the dPGS corona as a dark margin around the nanorods (Vonnemann et al., 2014).

2.11. Animal Models

Animal models in general try to reproduce the studied disease as closely as possible. Mice and rats are most widely because they are relatively cheap in maintenance and easy to handle. Additionally, mice and rats have high homology with the human organism, which makes them suitable for in vivo scientific research on human diseases.

For RA, it is important that the animal model relies on the same key pathophysiological steps towards the development of the disease. This involves the autoimmune inflammatory pathway through the activation of macrophages and T lymphocytes and the subsequent release of TNF-α and Interleukins, most importantly Interleukin 6.

To induce RA, murine models rely on collagens or antibodies. While collagen-induced arthritis results in an active immunization, antibody injection leads to passive immunization. Collagen-induced arthritis (CIA) is widely used both for rats and mice. It relies on the injection of collagen II as it is a main component of cartilage and soft tissue. It is typically combined with a pro-inflammatory component, that amplifies the immune response towards collagen II. One of the most widely used CIA protocols relies on the injection of bovine collagen II with complete Freund's adjuvant. Complete Freund's adjuvant consists of heat-killed mycobacteria tuberculosis, thus strongly boosting the immune response. For this model, usually DBA/1 mice are used as they can easily develop an appropriate immune response (Holmdahl, Jansson, Larsson, Rubin, & Klareskog, 1986). Ultimately, the injected animals develop an acute to subacute erosive polyarthritis within ~30 days with many similarities to human RA such as the production of rheumatoid factor and anticitrullinated peptide antibody. CIA models can also be used to study the effect of treatment for RA. Methotrexate and glucocorticoids have been proven to be effective treatment also for collagen-induced mice with arthritis (Schurgers, Billiau, & Matthys, 2011). Additionally, the course of the disease can be measured through clinical signs and clinical arthritis scoring systems. Imaging can be used to determine the severity of RA through assessment of bone lesions and inflammation of the joint.

Furthermore, a collagen antibody–induced arthritis (CAIA) can be used as a murine model for RA. Hereby, a variety of different antibodies targeting type II collagen is used for RA induction. The model also has strong similarities with human RA, such as synovitis and the development of bone damage. Moreover, the disease in CAIA proceeds very quickly with full arthritis 8 days after the initial injection (Khachigian, 2006).

3. Materials and Methods

3.1. Mouse Model

The government of Upper Bavaria approved the use of mice for our study (reference number 55.2-1-54-2532-179-11). The mice were treated in accordance with the local animal welfare committee of the medical faculty of the Technische Universität München. Overall, 39 male DBA/1 Mice from Janvier Labs, France, initially aged 7-8 weeks were used for the experiments. The collagen-induced arthritis (CIA) murine model was used as it is the most commonly used model for RA (Brand, Latham, & Rosloniec, 2007). An emulsion consisting of Freund's complete adjuvant and phosphate buffered saline (PBS) containing bovine type II at a 1:1 ratio was used to induce arthritis. Freund's complete adjuvant consists of mineral oil and heat-killed mycobacteria tuberculosis at a concentration of 1 mg/ml. As previously described by (Kamala, 2007) 20 microliters of this emulsion was injected below the left knee of each mouse. The animals received a booster injection after three weeks in the same way. After roughly two weeks first clear signs of arthritis like swelling, redness, and stiffness of the leg were visible. Within 25 - 30 days the mice developed arthritis. All animals were examined daily and specific symptoms such as swelling, redness and stiffness of the legs were graded in a ranking scale from 0 to 4 (0: no symptoms, 1: minor, 2: mild, 3: moderate, 4: severe symptoms respectively). Additionally, blood samples from each mouse were obtained once a week from the facial vein. Subsequently, the concentration of lymphocytes and granulocytes was determined. Furthermore, the ratio of lymphocytes to granulocytes was calculated as it is typically low in the acute phase of an inflammation and high in the chronic phase.

3.2. Therapy

A group of mice received an effective and typical treatment for the collagen induced arthritis model consisting of methotrexate and methylprednisolone. Alike to human RA, these drugs were shown to result in a less severe progression of the disease, more so if treated early (Dekkers et al., 2017). Through intraperitoneal injection (i.p.) the mice were administered 4,2 mg methylprednisolone acetate (Depot-Medrol, Pfizer) at 0,105 ml/kg (1:20), and 1 mg/kg methotrexate (MTX HEXAL, HEXAL AG) at 0,13 ml/kg (1:20).

3.3. MSOT contrast agents

3.3.1. dPGS-NIR contrast agent

The optical contrast agent “Mivenion 2012” was obtained from Mivenion, Berlin, Germany. The contrast agent is based on a fluorescent near infrared (NIR) dye connected to dendritic polyglycerol sulfate (dPGS). dPGS bind to P- and L-selectins - transmural proteins that are highly expressed on the surface of inflamed tissue. The dPGS-NIR has a specific absorption spectrum with peaks at 710 nm and 795 nm. The fluorescence emission peaks at 810 nm with a quantum yield of ~1%. 7.5mg/kg of the dPGS-NIR contrast agent was administered intravenously ~2h prior to the imaging experiments.

3.3.2. Gold Nanorods (AuNR)

In collaboration with Jonathan Vonnemann et al. from the Institute of Chemistry and Biochemistry at Freie Universität Berlin, Germany, imaging experiments with a contrast agent based on gold nanorods (AuNR) were performed. Hereby, dPGS is the active ligand for the functionalization of AuNR. The contrast agent was synthesized by Jonathan Vonnemann et al. as described in detail in the published paper (Vonnemann et al., 2014).

In brief, gold nanorods are coated in a CTAB double-layer and funtionalized using mPEG100-SH. Through amide coupling, thioctic acid functionalized dendritic polyglycerolsulfate (TA-dPGS) is synthesized from dPGS. In a last step, mPEG100-SH in the coat of the gold nanorods is replaced with TA-dPGS through thermally induced ligand exchange reaction resulting in dPGS-AuNR. dPGS-AuNR has a resonance band around 780 nm, thus allowing for its use as a MSOT contrast agent based on its specific light absorption characteristics within the near-infrared light spectrum. This contrast agent targeted inflamed tissue in the same way as dPGS-NIR - through binding to L- and P-selectins. For the imaging experiments, 5 mg/kg of dPGS-AuNR were injected intravenously into the animals. Imaging was performed at multiple timepoints after the injection starting immediately after the injection up to 24h thereafter.

Additionally, AuNR imaging experiments were performed with polyethylene glycol (PEG) instead of dPGS as the active ligand. PEG does not have an inflammation targeting mechanism and was used to evaluate the effectivity of the targeting process. For these experiments, 5 arthritis induced mice and one control mouse were used.

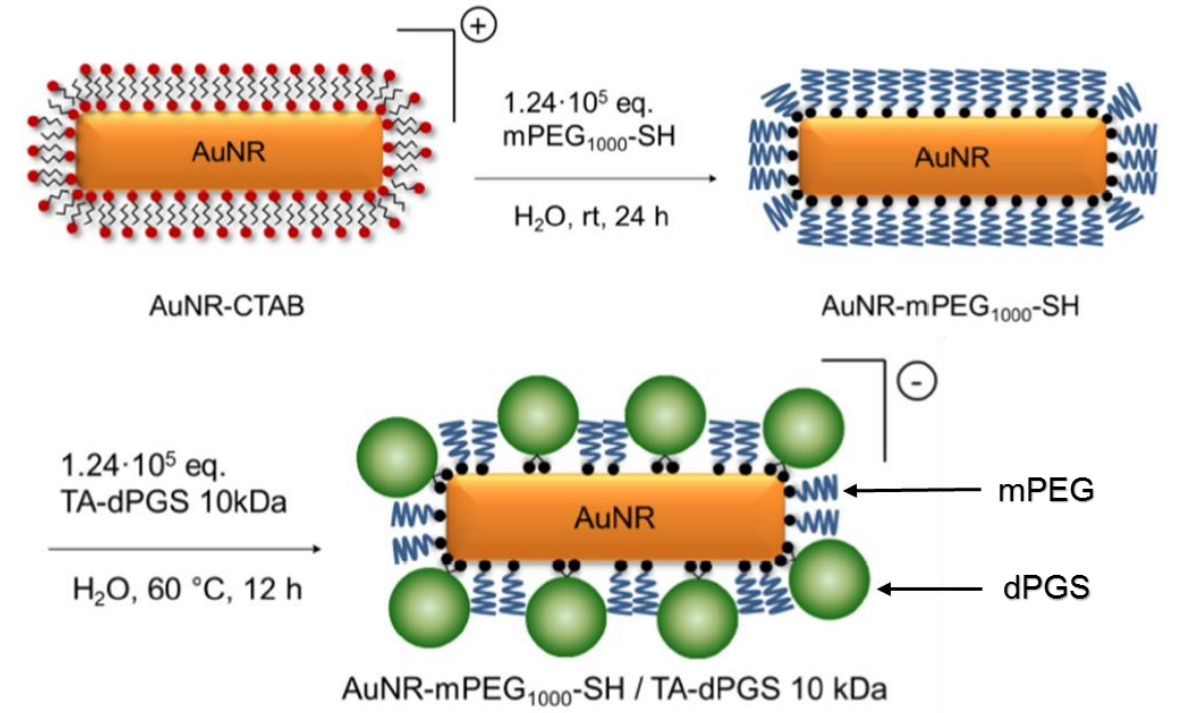

Figure 6: Schematic illustration of the AuNR-dPGS synthesis process: First, the CTAB coated gold nanorods were functionalized with mPEG. Then mPEG was partially replaced with dPGS through thermally induced ligand exchange reaction to obtain AuNR-dPGS (Vonnemann et al., 2014).

3.4. MSOT Imaging

The MSOT imaging experiments were performed in a real-time optoacoustic imaging system, as previously described by Ma et al. (2009). Accordingly, a Q-switched Nd:YAG laser with ~10 ms pulse duration and a 10 Hz repetition rate illuminated the target tissue within the tunable range of 680 nm - 980 nm. To allow for more evenly distributed light intensity, the fiber bundle was split into 10 output arms and illuminated the tissue in a semicircular fashion. The emitted ultrasound signal was recorded using a transducer with a central frequency of 5 MHz. The transducer consisted of 256 elements that were positioned circularly around the illuminated area to allow for tomographic image acquisition. The specimen was then placed on a moving stage to acquire images of different transverse planes. The specimen was enclosed in a thin clear polyethylene membrane. To ensure ultrasound transmission from the specimen to the transducer, imaging was performed in a 34°C water bath. During the image acquisition, the animals were anaesthetized by inhalation of 1.8% isoflurane. Images were obtained after 150 minutes after administration of the contrast agent injection as this results in the best contrast-to-noise ratio as shown in previous studies (Herzog et al., 2012) and confirmed for this study using multiple time points up to 240 min.

The entire lower body and hind legs of the mice were shaved to avoid light absorbance by the dark hair of the mice. Then, the mice were positioned in a standardized manner within the

MSOT device. Every limb and the head were fixated, and the hind legs were stretched symmetrically to facilitate optimal illumination of the rear joints. Images were obtained gradually in 0.5mm steps from the toes of the hind leg to the hip of both sides simultaneously. The imaging data was acquired using 30 averages per illumination wavelength and six different illumination wavelengths (700 nm, 730 nm, 760 nm, 800 nm, 830 nm, 860 nm). Using these illumination wavelengths, the main photoabsorbers oxyhemoglobin, deoxyhemoglobin, and dPGS-NIR, as well as dPGS-AuNR could be easily differentiated and identified.

For the imaging experiments to proof the validity of MSOT imaging findings and establish a staging protocol, MSOT imaging was performed at a mean 32 days (SD 2 days) after the induction of arthritis with 12 mice. For therapy monitoring experiments with 20 mice, the imaging experiments were performed 35 or 42 days after the induction of arthritis. The overall MSOT acquisition time per animal resulted in ~20 min.

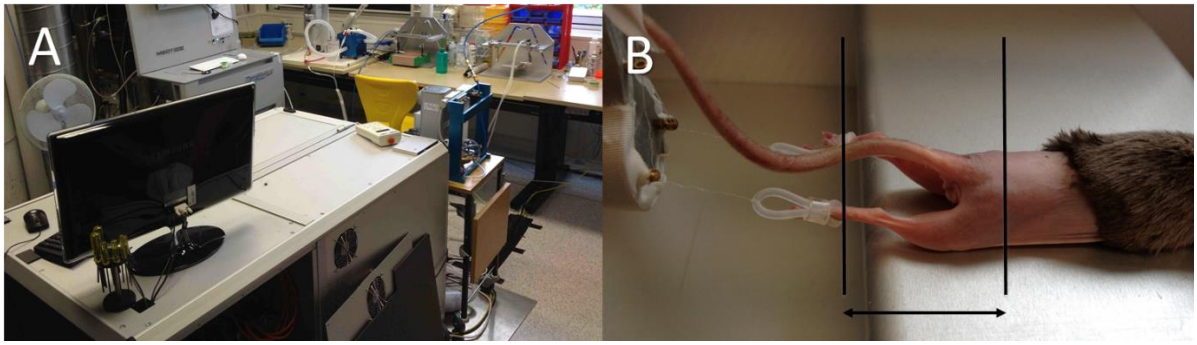

Figure 7: A: MSOT imaging setup. MSOT imaging system with monitor to adjust the imaging settings and to view preliminary live acquisition images. B: The mouse was scanned from below the ankle joint up to above the knee joint and was shaved within that area to avoid light absorbance by the fur.

3.5. MSOT Image Analysis

A model-based reconstruction process was used for the MSOT data as previously described by Rosenthal, Razansky, and Ntziachristos (2010) and Buehler et al. (2011). Spectral unmixing was performed based on spectral fitting by the least-squares method using the absorbance spectra of the contrast agent, oxygenated, and deoxygenated hemoglobin. As bone absorbance of the selected illumination wavelengths was not significant its contribution was not included in the analysis. The resulting data was then processed by a MatLab software with a custom-made script. For arthritis evaluation, axial images of both legs were used showing the joint region of knees or ankles.

To evaluate the MSOT imaging findings of arthritis, images were chosen that depicted the corresponding joints of both hind legs simultaneously. Specifically, the ankle and knee joints of the hind legs were evaluated. Within these images and based on their 800nm illumination characteristics, one region of interest was chosen for each of the two depicted corresponding joints of the left and right side respectively.

20% of the overall maximum value of the dPGS-NIR signal within each region of interest served as a signal threshold to minimize excess noise. Ultimately, the signal intensity values of the 25% pixels with the highest signal intensity were summed up to represent the overall value of the accumulation of the contrast agent on each side. To obtain an overall score of arthritic inflammation, the ratio of the arthritic left joint to the healthy right joint was determined. This ratio was calculated by subtracting the signal value of the right leg (R) from the signal value of the left leg (L) and dividing the resulting difference by the signal value of the left leg (L):

$$Relative\ signal\ difference\ of\ dPGS-NIR\ accumulation = \frac{L-R}{L}$$

To measure the increased blood flow in the inflamed joint area a threshold for normal blood circulation was determined. The amount of pixels with above threshold levels of deoxygenated and oxygenated hemoglobin signal was computed to represent the increase in blood circulation.

The imaging experiments were performed either 5, 30, or 42 days after the arthritis induction.

3.6. Magnetic resonance imaging (MRI)

Magnetic resonance imaging (MRI) was performed using a 1.5T clinical MR system (Achieva, Philips Medical Systems) with a surface coil. The animals were anaesthetized by inhalation of 1.8% isoflurane during the image acquisition. The mice were positioned in a standardized manner within the MRI device. Every limb was fixated and the hind legs were stretched. The surface coil was placed on the hind legs. 0,5 mmol/ml gadopentetat-dimeglumin (Magnevist, Bayer) was used as a contrast agent. 0,5 mmol/kg gadopentetat-dimeglumin was injected through a venous tail catheter immediately before T1 weighted contrast agent enhanced MRI. Localizer sequences were used to determine the area of the hind legs and the hip. The MRI sequences and MR image analysis protocols were adapted from the EULAR-OMERACT recommendations for RA imaging in humans (Østergaard et al., 2005). Sagittal MRI scans of this area were performed using a Proton Densitiy (PD) Spectral Presaturation with Inversion Recovery (SPIR) MRI sequence before contrast agent application. Sagittal T1-weighted MRI scan was performed before and after contrast agent application to evaluate contrast agent enhancement. The overall MRI acquisition time amounted to ~40 min.

The MR images were analyzed by an experienced radiologist blinded to the results from previous imaging findings and their respective groups. The imaging findings of each joint were graded in a ranking scale from 0-3 (0: no synovitis, 1: mild arthritis, 2: moderate arthritis, 3: severe arthritis) based on the scoring system OMERACT (Ostergaard et al., 2003). Thus, synovitis was defined as an area of the synovium that shows abnormal gadolinium enhancement, and an enlargement of the synovial membrane (Østergaard et al., 2005).

Figure 8: MR imaging setup using a human MRI system: The mouse was anesthetized with isoflurane and taped to boxes to avoid motion artifacts. A tail vein catheter allowed for contrast agent injection between the MR sequences. A surface coil was placed above the hind legs to improve MR image quality.

3.7. Histopathologic Analysis

Histopathologic analysis was performed in collaboration with Dr. Michaela Aichler and Prof. Dr. med. Axel Walch from the department for analytic pathology of the Helmholtz Zentrum München.

Following the imaging experiments, the animals were killed by cervical dislocation. The limbs were separated from the torso and the skin of the limbs was removed. Subsequently, the body was frozen using liquid carbon dioxide and then stored at -80°C. To verify the MSOT imaging findings ex vivo histopathologic analysis was performed using a fluorescent dye consisting of dPGS connected to a fluorescent indocarbocyanine conjugate (ICC). dPGS-ICC was acquired from Mivenion, Berlin, Germany. dPGS-ICC is a structural analog of the dPGS-NIR with an absorption and emission spectrum within the visible range. ICC has an absorption peak at 550nm and a fluorescence emission peak at 570nm. This allows for histopathologic analysis of the affected joints and tissue using a fluorescence microscope. 7.5mg/kg of the dPGS-ICC was administered ~2h before cryoconservation of the animals. The limbs of mice that were administered dPGS-ICC were fixed in formalin and decalcified using Osteosoft (Merck) following the manufacturer's instructions. The limbs were cut in 4µm slices. Additionally, the tissue was stained using hematoxylin and eosin. Afterwards, fluorescence imaging was performed using an Axio Imager Z1 upright microscope system (Carl Zeiss). The ICC component was identified using a 43 HE DsRed filter set (Carl Zeiss). Nuclei were detected with a Hoechst 33342 dye (Filter set 49 DAPI, Carl Zeiss).

The histopathologic analysis was performed by an experienced histopathologist blinded to the results from previous imaging findings and their respective groups. The histopathological findings were graded in a ranking scale from 0 to 3 (0: no changes, 1: few focal infiltrates, 2: extensive focal infiltrates, 3: extensive focal infiltrates invading the capsule).

3.8. Statistical Analysis

To show that MSOT is able to differentiate between different grades of arthritic inflammation, the mice were grouped into three different subsets according to the severity of their illness. The severity stages were defined as healthy, low inflammation, and high inflammation based on clinical symptoms, and MRI findings. The signal values representing the accumulation of the contrast agent were calculated for each group.

To study the effect of therapy in the MSOT findings, mice with and without effective treatment were compared based on their MSOT signal values. The mean value as well as standard deviation were calculated for each group, and the independent two-sample t-test was used for further statistical analysis. Additionally, for clinical grading the mean value and the standard deviation were determined based on the aforementioned ranking scale and compared using the two-sample t-test.

4. Results

4.1. Clinical Findings

In the first part of the experiments, all of the 12 induced mice developed some clinical symptom of arthritis such as swelling or redness of the limb, and stiffness of the joint. Furthermore, 6 of the 12 arthritis induced mice developed moderate to severe clinical symptoms with a clinical grade 2 or 3. In our collagen induced arthritis model, the left hind leg where the arthritis induction took place, developed swelling in all arthritic animals, while little to moderate clinical signs could be detected on other legs. These findings are in accordance with previously reported experiences with the collagen induced arthritis model (Caplazi et al., 2015). The grading score for arthritic mice had a mean of 1.58 with a standard deviation of 0.66. The blood samples showed typical findings of chronic inflammation with an increase in the lymphocyte to granulocyte ratio 30 days after the arthritis induction with a mean 9.9:1 and a standard deviation 8.6:1. In contrast, in a healthy control mouse neither clinical signs of arthritis nor a deviation from a normal lymphocyte to granulocyte ratio were observed.

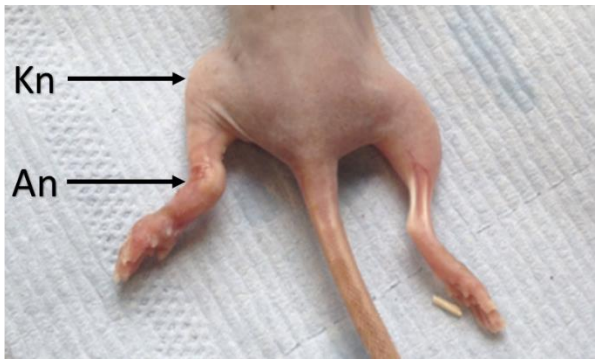

Figure 9: Mouse 34 days after the induction of arthritis. Overall the left leg was clearly swollen, especially the left knee (Kn), ankle (An) and the paw. In contrast, the right leg did not show clear swelling or redness. For imaging purposes, the hair was removed with depilatory cream.

4.2. MSOT *in vivo* Imaging Using dPGS-NIR

To evaluate the imaging data, images were generated based on spectrally unmixed optoacoustic signal of oxygenated and deoxygenated blood, as well as the dPGS-NIR contrast agent. These images were overlaid with imaging data at 860nm illumination wavelength as anatomical contrast because the optoacoustic signal is barely altered by the contrast agent and hemoglobin at that wavelength. This way, the accumulation of the contrast agent could be assessed and compared to the blood distribution. More specifically, using the oxygenated hemoglobin signal the location of arterial vessels could be detected. Conversely, the venous vessels could be determined with the signal of deoxygenated blood. Thus, the signal of the

contrast agent could be easily compared to venous and arterial vessels allowing for evaluation of the contrast agent extravasation process.

In first imaging experiments, we performed full imaging data acquisition at various timepoints after the injection of the dPGS-NIR contrast agent. The timepoints ranged from immediately after up until 240 min after the injection. At around 150 min, the contrast agent showed low signal in the vessels, yet high signal in the surrounding tissue of the joint. Therefore, the contrast agent had mostly extravasated and accumulated in inflamed tissue through binding to L- and P-selectins, while renal elimination of the contrast agent did not yet lead to decreased contrast enhancement at that timepoint. Thus, we concluded that 150 minutes after injection was the best time point to perform imaging experiments. These findings were in accordance with previously performed imaging experiments with this contrast agent (Herzog et al., 2012).

In the arthritis induced mice, a clear increase in the MSOT contrast agent signal within the joint area was observed showing the strong accumulation in the inflamed tissue. The increase consisted of at least > 35% for mice, where synovitis was confirmed through MRI. Conversely, in the healthy mice no significant increase was detected except for one limb of one healthy mouse. This resulted in a significant difference ($p = 0.023$) for the average signal in arthritic joints versus the average signal in healthy joints.

Furthermore, typical MSOT findings of arthritic mice could be observed. Firstly, swelling of the joint or the limb was easily identified in the anatomical 860 nm wavelength images as an increase in the overall tissue diameter. Secondly, an increase in blood flow could be detected through an increased signal of oxy- and deoxygenated hemoglobin. The amount of blood and the diameter of the blood vessels in the arthritic leg were increased. The saphenous vein was clearly enlarged with 2.6mm² lumen near the arthritic knee, as opposed to 0.65mm² in healthy animals. These findings are typical for inflamed tissue, and have been previously reported in collagen arthritis models (Ibarra et al., 2011).

Additionally, the area in which the inflammation targeting contrast agent accumulated was more extended in more severe cases of arthritis as identified by MRI. Also, the area showed higher average signal values for the contrast agent, meaning that not only the inflamed tissue or synovia was enlarged, but also the expression of L- and P-selectins was increased. This evidently resulted in higher contrast agent accumulation and thus indicating an overall increase in inflammatory activity. Using 3-dimensional reconstruction, the extent and severity of the inflammation around the joint was more easily observable. The arthritic legs showed high accumulation of the contrast agent in the inflamed joint and as well as in the surrounding soft tissue, whereas a healthy leg only showed low accumulation in the joint and barely any accumulation in the vicinity of the joint. Finally, all mice displayed significant contrast agent accumulation in the bladder as expected because of the renal excretion route of the contrast agent.

To allow for a standardized and objective way to evaluate and compare the imaging findings and the severity of arthritis, a customly developed quantitative analysis protocol was used. Thereby, the joints are compared regarding their respective enlargement of inflamed tissue and their signal values of the contrast agent. The ratios of the left and the right joint values were calculated to compare the inflammation in the joints. The contrast agent highly accumulated in inflamed joints resulting in high dPGS-NIR signal differences. In the exemplary case of severe arthritis as shown in figure 10, a 71% dPGS-NIR signal difference in the knee and a 600% signal difference in the ankle was recorded. The mean difference of contrast agent accumulation for all arthritic mice was 48% with a standard deviation of 11%. In the images of healthy control mice, the different joints were visually very similar. Using the standardized protocol only a low difference in the contrast agent accumulation of the joint could be determined. Overall, the signal intensity difference was below 30% in every healthy animal with a mean of 20% and a standard deviation of 17%.

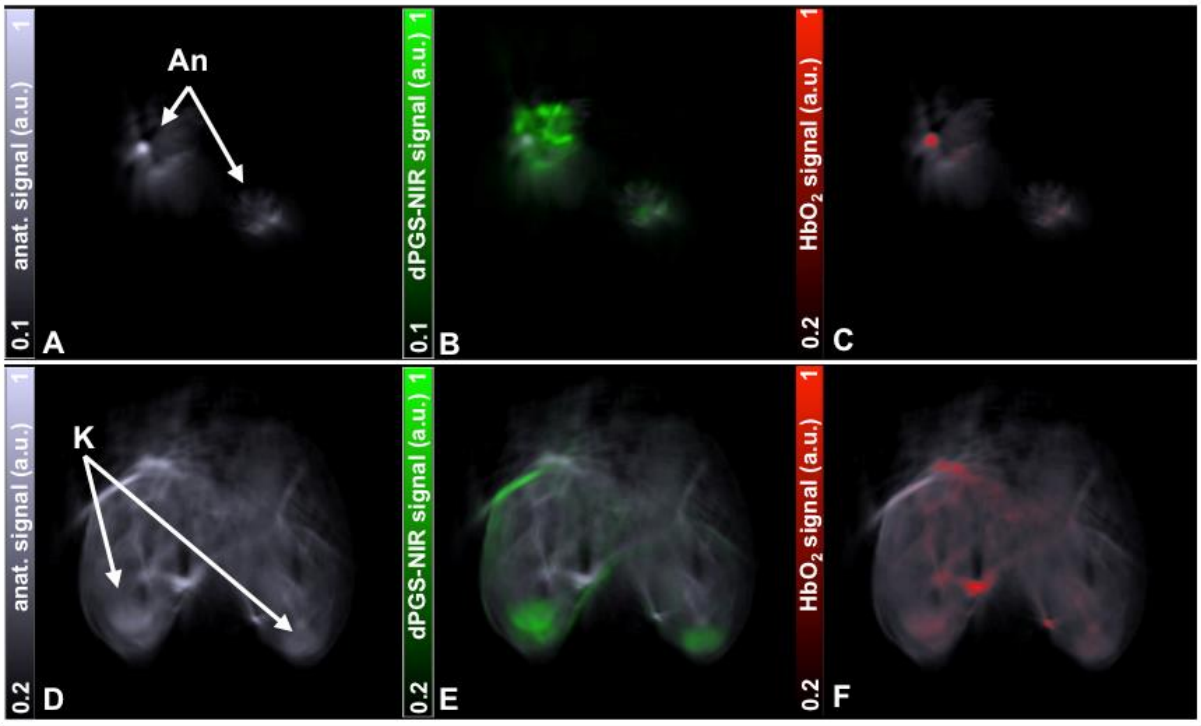

Figure 10: Multispectral optoacoustic imaging of a mouse ankles and knees at an advanced stage of arthritis using dPGS-NIR as a contrast agent. (A) Ankle (An) MSOT image acquired at 860nm illumination wavelength for anatomical contrast. (B) Overlay of the dPGS-NIR MSOT signal on the anatomical image. (C) Overlay of the oxygenated hemoglobin MSOT signal on the anatomical image. (D, E, F) is the same series of images but acquired at the knee joint. The left ankle is severely enlarged with very high signal intensity values for dPGS-NIR, thus the contrast agent strongly accumulated in the inflamed joint. The images for hemoglobin additionally revealed a strong increase in perfusion of the left ankle. The left knee (K) joint also showed strong contrast agent accumulation, while the right knee joint showed more moderate accumulation.

4.3. MRI and Association with Clinical Findings

MRI was performed at the same timepoint as MSOT imaging for each mouse. Sagittal MRI scans of the knee and ankle joints of the hind leg were obtained before and after contrast agent injection. The main MR finding in mice with arthritis was synovitis visible through synovial contrast agent enhancement. Moreover, soft tissue inflammation and tissue swelling in the area surrounding the joints could be observed. Some mice showed bone edema and bone erosions, typical findings for a more severe stage of RA. Pathological MRI findings were associated with evident clinical symptoms of the mice like swelling, redness or stiffness of the joint. The grade of the synovitis was assessed similarly to RAMRIS based on contrast agent enhancement. Overall, MR images were graded from no arthritis (0) to severe arthritis (3) represented in scores from 0 to 3. The mean score for arthritic mice was 1,5 with a standard deviation of 0.67.

Based on the clinical findings and the MR imaging results, the mice were grouped into three different subsets of mice depending on the degree of inflammation of the joint. The subgroups consisted of mice with no inflammation, low inflammation, and high inflammation, respectively. The grading score for all healthy control mice was 0, thus no findings indicative of inflammation could be seen. Pearson correlation coefficient between the clinical grading score and the MR grading score was 0.93, implying a strong correlation between clinical observation and MRI imaging results.

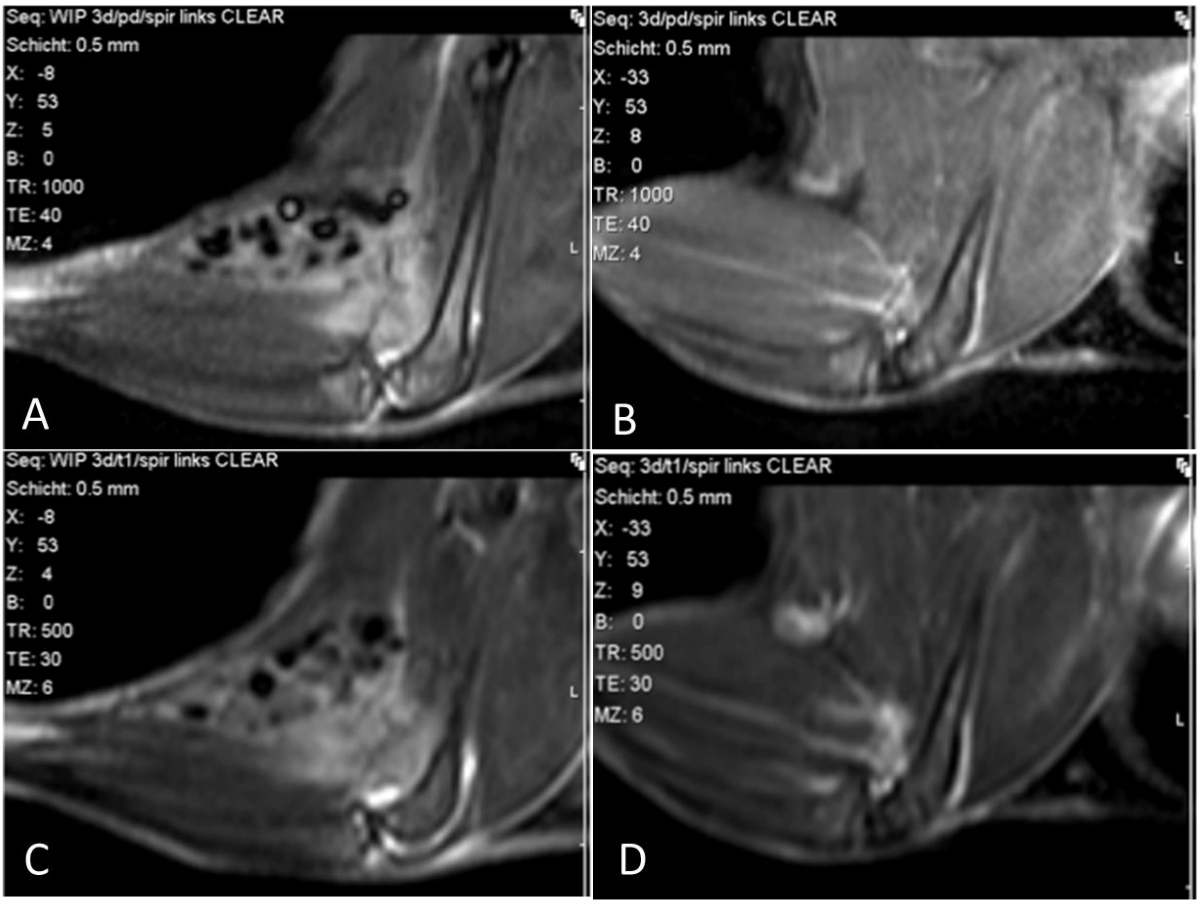

Figure 11: A, C: MR images of an arthritic knee joint before (A) and after (C) contrast agent injection: Hyperintense synovial structures after contrast agent injection represent synovitis. Hyperintense structures near the joint was inflamed soft tissue. B, D: MR images of a healthy control mouse before (B) and after (D) contrast agent injection: no increase in the intensity of the synovial signal after contrast agent application implied the absence of a synovitis. No alterations in the signal value of the surrounding soft tissue was visible.

4.4. Histopathologic Analysis

Using Hematoxylin and Eosin staining, the joint region of the ankle and knee of both hind legs were analyzed histopathologically. In arthritic legs typical findings for arthritic inflammation could be observed as shown in figure 12B: Enlargement of the synovia, expanded synovial space, erosion of the cartilage and bone. Furthermore, large inflammatory infiltrates could be identified in the whole joint region and specifically in the capsule. Fluorescence microscopy was performed with dPGS-ICC and DAPI. In arthritic joints, strong accumulation of dPGS-ICC in the joint was observed. As demonstrated in figure 12D, dPGS-ICC accumulated in the synovia and the bone representing synovitis and bone edema, respectively. Mild accumulation could be observed in the surrounding soft tissue of the joint, implying an overall inflamed soft tissue in the vicinity of the joint. Overall, this indicated that L- and P-selectins were highly

expressed in the inflamed joint tissue. These results showed the same accumulation pattern as the MSOT imaging results using dPGS-NIR and AuNR-dPGS. Thus, we could confirm the accumulation of the contrast agents in the joint as seen in vivo through MSOT. In healthy mice, however, a normal synovia without inflammatory infiltrates was observed as seen in figure 12A. Bone and cartilage structures appeared to be intact without bone erosion, bone edema, or pathological alterations to the cartilage. Moreover, healthy mice showed only sparse accumulation of dPGS-ICC in the joints as demonstrated in figure 12C.

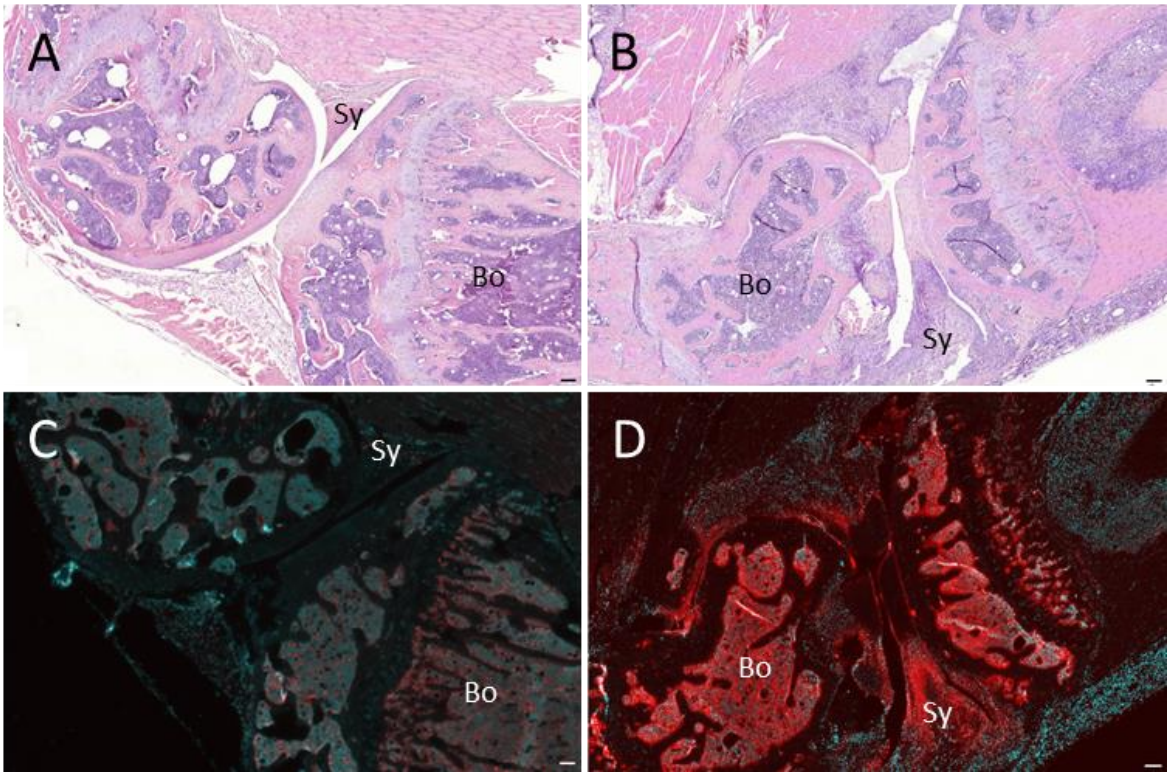

Figure 12: HE, 50x, SB 100 µm, Fluorescence, 25x, SB 100 µm (dPGS-ICC = red; DAPI = blue), A: Hematoxylin and Eosin stain of a healthy knee joint, B: Hematoxylin and Eosin stain of an arthritic knee joint with large inflammatory infiltrates in the synovial compartment (Sy) and the bone (Bo), representing typical findings for severe RA, C: Fluorescence image of healthy knee joint (A), D: Fluorescence image of arthritic knee joint (B): Evident accumulation of dPGS-ICC in the bone (Bo) and synovia (Sy) caused by inflammation of the bone and synovia.

4.5. Healthy Mice

In the images of healthy control mice the different joints were visually very similar, as shown exemplary in figure 13. Furthermore, the amount of blood and the diameter of the blood vessels was not increased, indicating normal blood flow levels. The lumen of the saphenous vein near the knee was also not increased and similar on both sides with 0.65mm² on the left and 0.59mm² on the right.

Similarly to MSOT, the MR images of healthy control mice did not reveal any arthritic findings like synovitis, bone edema, or swelling.

Histopathologic analysis of the healthy mice with hematoxylin and eosin displayed normal joints without inflammatory infiltrates and normal synovias without pathological enlargement. Fluorescence microscopy showed lower and more diffuse contrast agent accumulation in the joint. In the images of healthy control mice, the different joints were visually very similar. Using the standardized protocol only a low difference in the contrast agent accumulation of the joint could be determined. Overall, the signal intensity difference was below 30% in every healthy animal with a mean of 20% and a standard deviation of 17%.

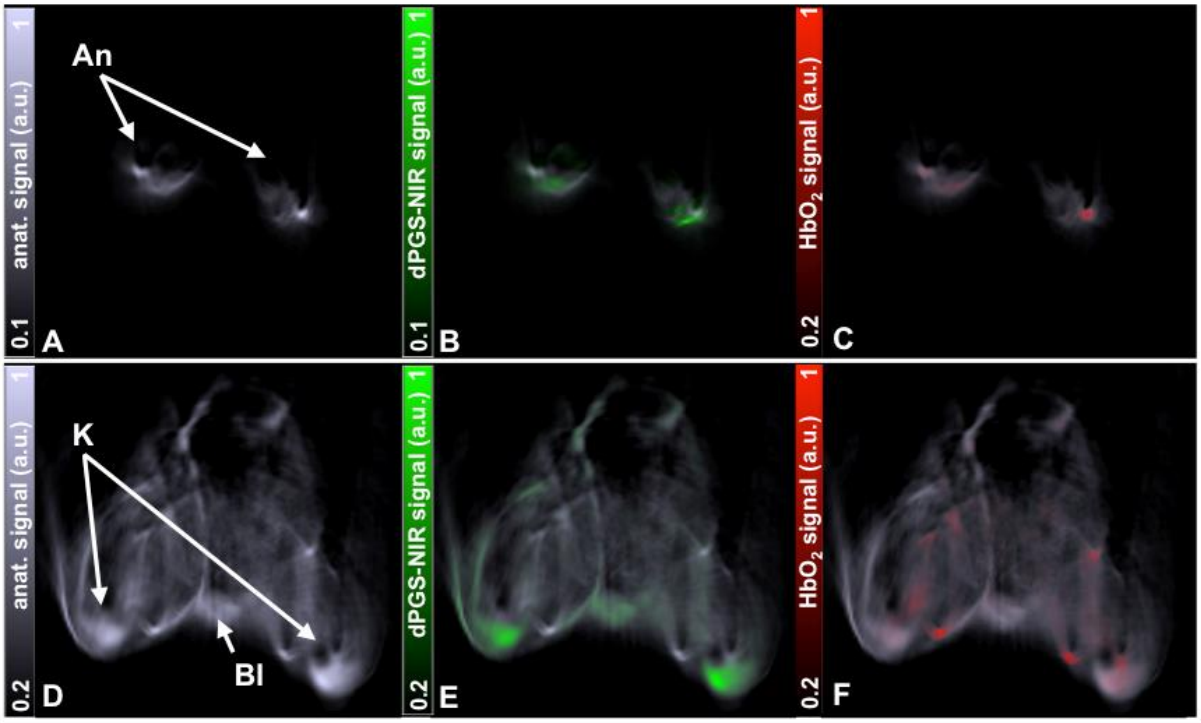

Figure 13: MSOT imaging of a healthy mouse using dPGS-NIR as a contrast agent. (A) Ankle (An) MSOT image acquired at 860nm illumination wavelength for anatomical contrast. (B) Overlay of the dPGS-NIR MSOT signal on the anatomical image. (C) Overlay of the oxygenated hemoglobin MSOT signal on the anatomical image. (D, E, F) is the same series of images but acquired at the knee (Kn) joint, with a part of the bladder (Bl) being visible. In healthy mice low and uniform accumulation of the contrast agents in the joints could be observed.

4.6. Staging of RA with MSOT Imaging using dPGS-NIR

To proof the validity of the MSOT findings, we compared the MSOT findings to MRI, clinical examination, and histopathologic analysis. Hereby, 12 mice were grouped in three different subsets according to the severity of their arthritis: no inflammation, low inflammation, high inflammation. These stages were defined by their MR findings and their clinical findings. Then, the MSOT findings of these groups were systematically compared. Accordingly, in joints where MSOT imaging did not reveal increased contrast agent accumulation, their corresponding MR images and clinical findings were also devoid of inflammatory signs such as synovitis (grade 0), or redness and swelling. In this group, the MSOT signal showed barely any difference between the corresponding joints of both hind legs, indicating a similar amount of contrast agent accumulation. In joints with low inflammatory activity, MSOT showed a mild increase in contrast agent accumulation, while MR findings revealed mild to moderate synovitis (grade 1-2). These animals had clear, but limited clinical signs of arthritis, like moderate swelling and redness of the affected joint. The mean MSOT signal difference was almost 50% between the two knee joints of the hind legs for mice with low inflammation with a standard deviation of 7%, demonstrating considerable accumulation of the contrast agent in the arthritic joint. When the joints of the animals were identified as highly inflamed, more severe synovitis was visible in MR images (grade 2-3) and more severe clinical signs as severe swelling and stiffness of the affected joint were evident. These mice showed strong accumulation of the contrast agent in MSOT as the mean signal difference of the joints was above 70% with a standard deviation of 15%.

Overall, the calculated differences were significant and the standard deviation low enough to classify the mice according to the severity of their arthritis ($p = 0.023$). This way, we could differentiate mice with no inflammation from mice with low and high inflammation.

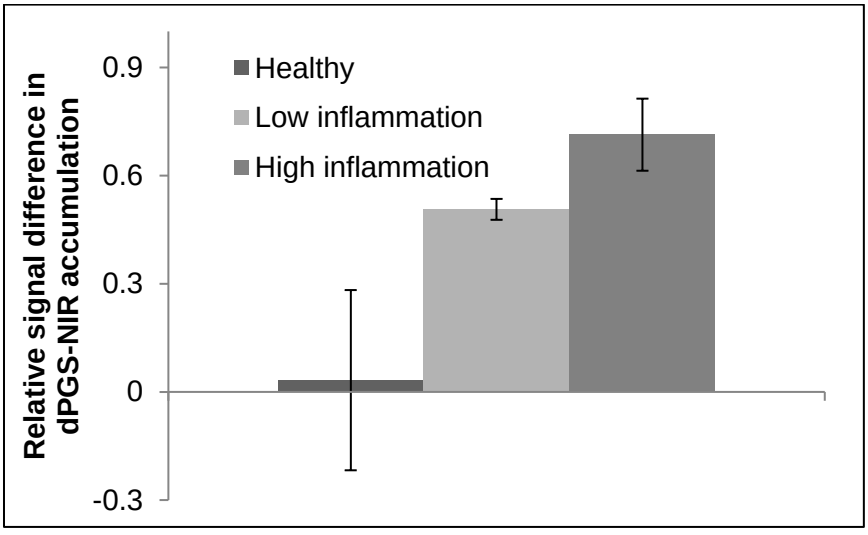

Figure 14: Difference in the dPGS-NIR signal between the two sides of the joint of animals based on their inflammation grade (Healthy, low and high inflammation). The inflammation grade was determined by clinical examination and MR imaging results. The group of mice identified as healthy on MSOT

showed no visible signs of inflammation and a normal blood cell count. The group of mice with low inflammation had a milder synovitis and a distinctly altered blood cell count. The group of mice with high inflammation showed more severe synovitis and a low lymphocyte:granulocyte ratio which are typical findings for severe RA. Bars represent the mean value ± standard deviation for the difference in dPGS-NIR accumulation between the two sides of the legs.

4.7. Therapy Monitoring with MSOT Imaging using dPGS-NIR

To understand the effect of appropriate therapy on MSOT imaging findings and the implication of those findings for the efficacy of the therapy, we performed imaging experiments at different timepoints after the induction of arthritis for mice with and without therapy. We closely monitored the clinical signs for RA to evaluate one aspect of the severity of the disease, and its development over time. Appropriate therapy should limit the inflammation in the joint and the severity of clinical signs. Ultimately, early signs in MSOT imaging of a dampened inflammatory process could translate into less severe clinical symptoms at the later stages in the development of RA. Additionally, findings of MSOT imaging were compared to MRI and histopathology for each mouse to validate those findings. The imaging experiments were performed on 5 days, 35 days, and 42 days after the induction of arthritis using 20 animals overall. 5 days after the induction no clear signs of a RA were observed in both mice with and without therapy. After 35 days clear signs of the disease were visible in 2 mice with therapy and 6 mice without therapy. Finally, after 42 days all mice developed clear arthritis.

At day 5 the mean difference was considerably low with a mean signal difference with 14% (SD=15%) for mice without therapy, and 17% (SD=9%) with therapy, and 15% (SD=12%) as a mean value for both groups together. At this timepoint, a very limited local inflammation was possibly caused by the arthritis induction, resulting in low accumulation of dPGS-NIR in the area of the joint as observed in 1 animal. Generally, however, the signal value, was low at day 5. 32 days after the induction, the mean signal value for mice without therapy increased to 38% (SD=48%), while the mice with therapy did not show increase with a value of 17% (SD=10%). The standard deviation was considerably higher in the first group as half of the mice developed more severe cases of arthritis with high dPGS-NIR contrast agent accumulation, while others showed more moderate arthritic inflammation with lower dPGS-NIR accumulation. At day 42, the mean value for mice without therapy remained constant at 38% while the standard deviation decreased to 16%. The signal value for mice with therapy increased to 24% (SD=27%). Some mice did not develop as severe arthritis as others, shown by high levels for standard deviation at the specific timepoints. Additionally, the limited number of mice at each timepoint did not to allow for more reliable results with lower levels of standard deviation.

Overall, the mean MSOT values were lower for treated mice compared to untreated mice at 35 and 42 days after the RA induction. While the dPGS-NIR accumulation was constant for

untreated mice at 35 compared to 42 days after the induction, mice that underwent therapy showed a further increase within that time span. As dPGS visualizes one of the key elements for leucocyte extravastation, it can directly show the effect of therapeutic inhibition of inflammation. Glucocorticoids and MTX both significantly dampen the immune response and the expression of L- and P-selectins, thus, as expected the accumulation of dPGS-NIR was lower in treated mice compared to untreated mice.

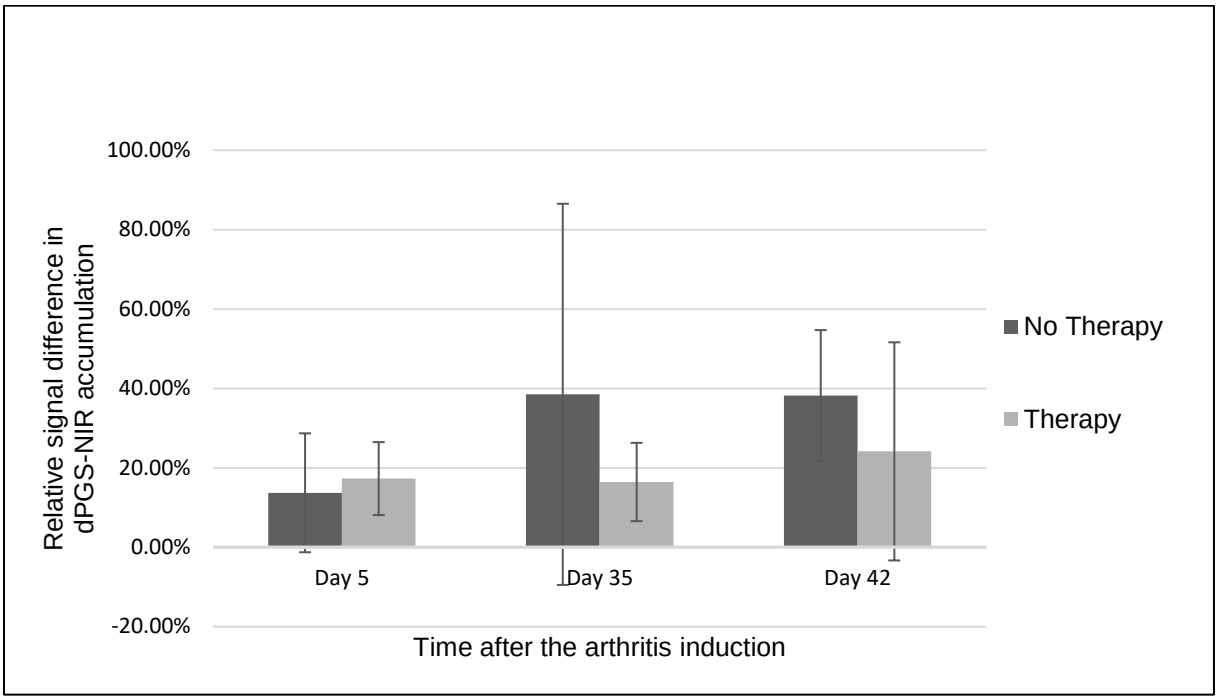

Figure 15: Relative dPGS-NIR signal difference of mice at the three different timepoints with and without therapy. The accumulation of the contrast agent increased over time in mice with therapy, while mice without therapy showed a strong increase from day 5 to day 35, but no additional increase towards day 42.

Accordingly, we analyzed the clinical symptoms of the mice at each time point using the clinical grading score. We calculated mean and standard deviation for each time point. At day 5 none of the mice had clinical symptoms of arthritis. After 35 days, the mean clinical grading score increased to 1,0 with and to 1,1 without therapy. After 42 days, the score increased even further for both groups to 1.3 and 1,5 without therapy.

Altogether, an increase in the clinical symptoms could be observed throughout both groups and all timepoints, implying the progression of the disease over time to its full extent 42 days after the induction. However, treated mice showed more severe clinical symptoms than untreated mice, thus implying that therapy was indeed effective. In addition, the difference in the clinical severity of the disease between mice with and without therapy increased from 35 days to 42 days after the induction. This represented a growing effect of the therapy over time and over the course of the disease.

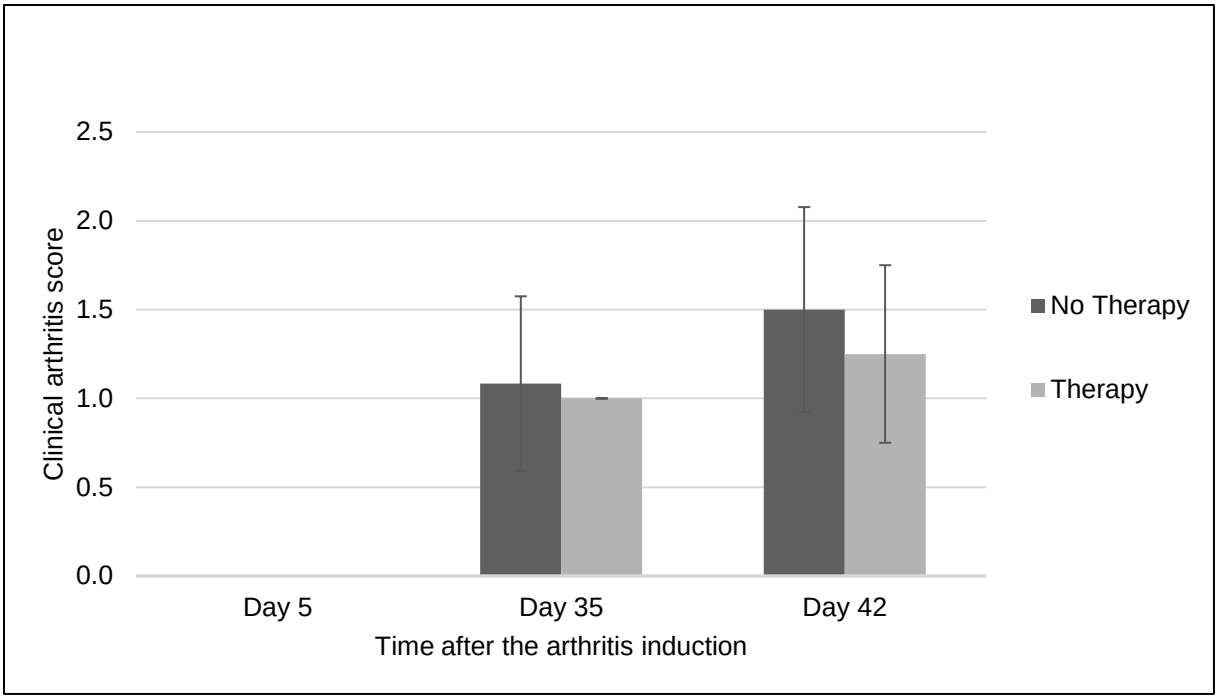

Figure 16: Clinical scoring of the mice at the three different time points with and without therapy. Score represents a combined assessment of swelling, redness, and stiffness of the joint. No clinical findings in the mice at day 5 as signs of arthritis were yet to develop. Overall, a constant increase of clinical symptoms over all timepoints and both groups. However, mice without therapy showed more severe clinical symptoms both 35, and 42 days after the induction.

Overall, a difference between mice with and without therapy was more clearly observable in MSOT imaging than by clinical scoring at 35 days after the arthritis induction. This could indicate that MSOT imaging can identify the effect of appropriate therapy before clinically detectable symptoms of the disease occur. The pearson correlation coefficient between MSOT grading and clinical grading was 0,36.

4.8. MSOT Using dPGS Coated Gold Nanorods (AuNR-dPGS)

In preliminary phantom studies, the MSOT absorption characteristics of AuNR-dPGS were first established to allow for an accurate and valid calculation for the spectrally unmixed AuNR signal. This study showed that only a very low optical density (OD) is necessary to identify the AuNR based contrast agent.

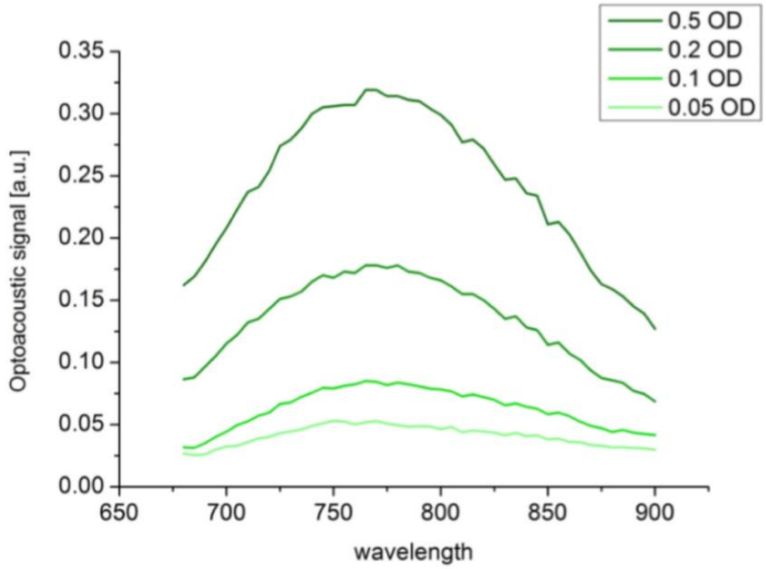

Figure 17: Optical density of AuNR-dPGS: Through a MSOT phantom study with AuNR-dPGS as the contrast agent the optoacoustic signal was determined depending on the illumination wavelength at different optical densities OD. AuNR-dPGS could be detected as low as 0.05 OD (Vonnemann et al., 2014).

For in vivo imaging, MSOT was performed 4h after intravenous injection with gold nanorods either targeted AuNR-dPGS or untargeted AuNR-PEG. MSOT images were calculated for the absorption characteristics at an illumination of 800nm for anatomical contrast (Figure A and D). For the evaluation of the localization and accumulation of AuNR-PEG, and AuNR-dPGS, their spectrally unmixed signal was calculated. The visualized signal intensity was overlaid with the image for anatomical contrast to allow for anatomical representation, as well as colocalization and assessment of the accumulation the of the contrast agent (Figure B and E). To assess the vascular component of the contrast agent signal, the spectrally unmixed oxygenated blood signal was visualized as well (Figure C and F). This way, a detailed visualization and assessment of the AuNR based contrast agent was possible as depicted in the figure below. The MSOT imaging findings were then confirmed through MR imaging, clinical observation, and histopathologic analysis.

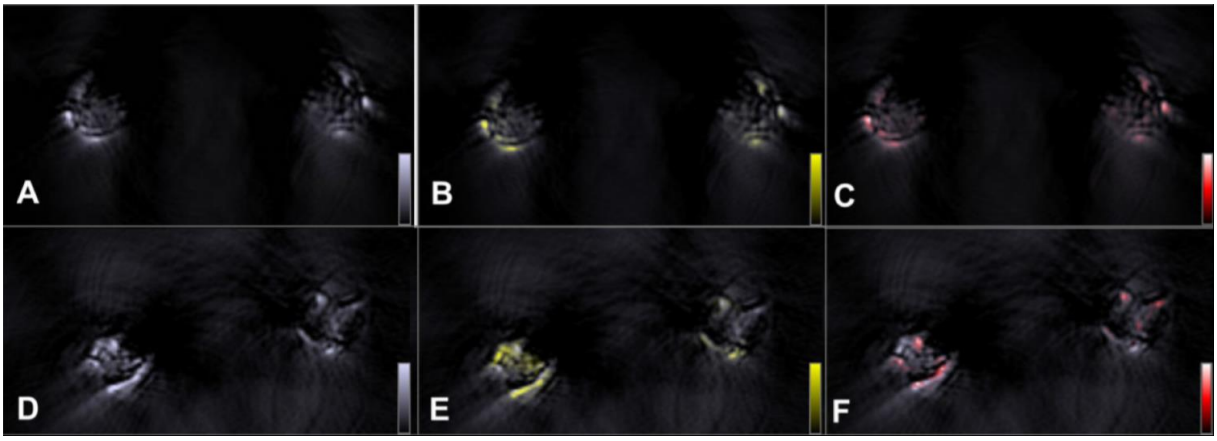

Figure 18: MSOT images from the ankles of two different mice using AuNR-PEG (A, B, C) and AuNR-dPGS (D, E, F) as contrast agent. A: illumination at 800nm for anatomical contrast, B: Spectrally unmixed AuNR-PEG signal (yellow) overlaid with "anatomical image", C: Spectrally unmixed oxygenated hemoglobin signal (red) overlaid with "anatomical image", D: illumination at 800nm for anatomical contrast, E: AuNR-dPGS signal (yellow) overlaid with "anatomical image", F: oxygenated hemoglobin signal (red) overlaid with "anatomical image". While AuNR-PEG shows low to moderate signal intensities in the ankles of both sides uniformly, the targeted AuNR-dPGS clearly accumulated in the left ankle of the mouse.

Neither AuNR-PEG nor AuNR-dPGS showed in vivo aggregation because otherwise the optoacoustic signal would have been significantly altered, and thus not allowing for clear visualization in MSOT through spectral unmixing. As expected the two mice injected with AuNR-PEG did not show clear accumulation in the inflamed tissue. In both mice the signal difference between the corresponding joints of the hind legs was less than 10%. Without an inflammation targeting mechanism AuNR-PEG did not extravasate and accumulate as strongly in inflamed tissue. AuNR-PEG was mainly localized in blood vessels as confirmed by colocalization of oxygenated and deoxygenated blood signal through spectral unmixing. In contrast, the four mice injected with AuNR-dPGS showed clear accumulation of the contrast agent in the arthritic joints as expected since AuNR-dPGS relied on the same inflammation targeting mechanism as NIR-dPGS. Accordingly, similar contrast agent dynamics and contrast agent accumulation in arthritic joints and inflamed tissue was expected. At the time the imaging was performed, most of the AuNR-dPGS had already extravasated from the blood vessels and accumulated in the inflamed area. The mean signal difference of AuNR-dPGS between the corresponding joints of the arthritic left leg and the right leg was ~70% with a standard deviation of ~30%.

5. Discussion and Conclusion

5.1. Overview

In this study we used two inflammation targeting contrast agents to visualize rheumatoid arthritis (RA) in the joints in a murine model using multispectral optoacoustic tomography (MSOT). The contrast agents were based on dendritic polyglycerol sulfate (dPGS), which selectively binds to inflammatory surface proteins, thus allowing for direct visualization of inflammation. MSOT imaging findings were compared to MR imaging, clinical findings, and histopathologic analysis. Using a dPGS based near infrared dye (dPGS-NIR) as contrast agent, MSOT was able to differentiate mice without inflammation from mice with low, and high inflammation, respectively. In addition, MSOT was also able to detect inflamed joints with a different contrast agent based on gold nanorods (AuNR) coated with dPGS. Furthermore, we studied the effect of appropriate therapy towards MSOT imaging findings. Clear differences were observed when we compared mice that received therapy to those that did not. Thus, MSOT could be used as a tool to monitor the efficacy of therapy.

5.2. Mouse Model for Rheumatoid Arthritis

Overall, using the collagen induced arthritis (CIA) model with active immunization, the mice reliably developed arthritis within ~30 days. However, the differences in the severity of the disease were substantial, and larger than in the collagen antibody–induced arthritis (CAIA) model with passive immunization. However, for studies regarding the efficacy of appropriate therapy a CIA model was more suitable as medication inhibits the production of antibodies against collagen II and thus the development of the disease. In contrast, CAIA relies on the direct injection of antibodies, so anti-inflammatory and immune-suppressant drugs have a weaker effect (Khachigian, 2006).

The CIA arthritis induction was performed on the left leg. While some studies report a uniform development of arthritis in the different joints regarding the extent of the inflammation, we observed that mainly the left leg developed severe arthritis, while most of the joints of other limbs were only mildly inflamed or not inflamed at all. These differences in the development of arthritis in the CIA model have previously been reported. The same CIA protocol resulted in considerable differences in different studies regarding the distribution and uniformity of arthritic joints (Nandakumar & Holmdahl, 2007).

The therapy consisting of methotrexate and methylprednisolone has been shown to be effective in a CIA model (Dekkers et al., 2017). However, the overall small timeframe of 42 days in this study limited the therapeutic potency of the medication and might not have reached its full extent. Thus, the effect of therapy on the murine model might be weaker and the

differences between treated and untreated group lower, as previously reported by other studies (Ortendahl, Schettler, & Fries, 2000).

5.3. dPGS-NIR as Contrast Agent

The inflammation targeting dPGS-NIR dye showed clear accumulation in the inflamed area 150 min after the injection while no substantial accumulation was observed in healthy joints. The accumulation of the contrast agent in inflamed tissue could be confirmed histopathologically, indicating that the contrast agent successfully bound to L- and P-selectins. These findings are in accordance with a study that used MSOT to visualize myocardial infarction through MSOT. In this study dPGS-NIR also showed accumulation in inflamed tissue that could be confirmed histopathologically (A. Taruttis et al., 2013). Accordingly, the study concluded that dPGS-NIR was a powerful inflammation targeting contrast agent with high validity for optical imaging applications. As reported in various other imaging studies, dPGS-NIR did not show any signs of toxicity (Boreham et al., 2015).

In clinical practice, the use of a contrast agent such as dPGS-NIR would require critical assessment of risks and benefits. Likely, as a routine diagnostic and as a first imaging step towards the evaluation of RA the application of such a contrast agent might not be appropriate. However, for specific questions and a more detailed visualization of the extent of an arthritic inflammation its use might be justified. This could allow for an earlier diagnosis of arthritis in cases where anatomical visualization of the joint is inconclusive.

5.4. AuNR-dPGS as Contrast Agent

The main aim of the research using AuNR as an in vivo MSOT contrast agent was to show the feasibility of a targeted optical imaging contrast agent based on gold nanorods. We were able to show that dendritic polyglycerolsulfate functionalized gold nanorods could be used as a contrast agent to accurately visualize inflammation through MSOT in a murine model for RA. PEGylated gold nanorods AuNR-PEG were previously used in other imaging studies. As expected, AuNR-PEG did not strongly accumulate in inflamed tissue without an inflammation targeting mechanism. In contrast, AuNR-dPGS showed clear differences in the accumulation between healthy and inflamed joints, thus AuNR-dPGS could also also be used as a contrast agent for the diagnosis of arthritic joints. These results indicate that the essential factor for the accumulation of the contrast agent in the arthritic joints lies in the inflammation targeting properties of dendritic polyglycerol sulfates. Without this aspect, diagnosis and staging of arthritic inflammation would be more difficult because it would be depended on other effects of inflammation such as increase in vascularization, blood circulation, and enhancement of unspecific contrast agent.

In addition, gold nanorods can be used in a theranostic approach, allowing for simultaneous diagnostic and therapeutic procedures as dPGS already has anti-inflammatory properties. Furthermore, targeted drug therapy could be developed with gold nanorods as loaded drug vehicles. Under direct visualization through MSOT, the drug release could be triggered through specific laser light pulses, as described by Guerrero et al. (2014).

One key aspect and limitation for the use of functionalized gold nanorods as contrast agent is their toxicity, particularly as the toxicity varies greatly depending on the coating. The toxicity of AuNR-dPGS was investigated through in vitro experiments using umbilical vein endothelial cells. While gold nanorods with CTAB coating (AuNR-CTAB) resulted in high in vitro cell toxicity, PEGylation (AuNR-PEG) resulted in a 40 times lower cell toxicity. AuNR-dPGS showed significantly less toxicity than CTAB coating, though it was mildly more toxic than PEG. At concentrations < 5nM, AuNR-dPGS did not result in any cell toxicity (Vonnemann et al., 2014). Other studies showed comparable results regarding the toxicity of functionalized gold nanorods (Rayavarapu et al., 2010). However, the accurate assessment of the cell toxicity in vivo and the pharmacokinetics of AuNR-dPGS requires further research. Furthermore, the degradation and potential side effects of this compound would have to be thoroughly studied prior to a more widespread use and a potential human implementation.

5.5. Analysis Protocol for dPGS-NIR

The development of a standardized protocol for the image analysis was an effort to achieve a more user-independent and quantifiable assessment of the extent of arthritic inflammation through MSOT. For this image analysis protocol both the size of the inflamed tissue as well as the signal intensity of the contrast agent in the inflamed area was taken into account. A high signal intensity implies a strong expression of the inflammatory surface proteins L- and P-selectin and thus a higher degree of inflammation. An increase in the size of the inflamed soft tissue in the joint, such as an enlargement of the synovia, is also a common pathologic alteration that signifies the severity of arthritic inflammation.

Because the threshold level for noise was established beforehand the results of the measurements were only influenced minimally by the user-dependent selection of the region of interest (ROI). Moreover, the summation of the dPGS-NIR signal intensity for each pixel within the ROI allowed for the quantification of the size of the inflamed tissue through the number of pixels, as well as an assessment of the degree of inflammation through the signal intensity of each pixel. One limitation of the MOST imaging technique so far lied within the unstable pulse energy levels. The system could not reliably illuminate the tissue with a constant laser pulse energy over a longer period of time. While the laser pulse energy is usually stable enough to allow for comparison within the MSOT measurements of one animal, it does not allow to universally compare the optoacoustic signal intensities of different animals at different

time points. However, to allow for an objective and quantifiable comparison of arthritic inflammation between mice at different time points, we calculated the relative signal difference of the joints between the left and the right leg. As the right leg was usually not at all affected by arthritic inflammation, the signal intensity value of the joint of the right leg served as a baseline measurement. This way, arthritic inflammation could be accurately and reliably assessed with results that were comparable to those provided by MRI.

Overall, this analysis protocol allowed for an objective way to quantify the arthritic inflammation without relying on the subjective evaluation of the joint structures by eye. Generally, subjective assessment can surely be helpful, and allow for colocalization in other imaging modalities such as ultrasonography, MRI and radiography. However, a wide range of current radiologic guidelines try to objectify image assessment for specific diseases. Using this image analysis protocol, the quantitative image results were only based on the selection of the joint as the region of interest, thus allowing for a mostly user-independent assessment of the extent of arthritic inflammation.

5.6. Results of dPGS-NIR

We wanted to investigate whether MSOT with dPGS-NIR dye as an inflammation targeting contrast agent was able to identify arthritic inflammation and differentiate different grades of inflammation. Additionally, we wanted to compare MSOT imaging findings with MRI, histopathology, and clinical examination. Therefore, we compared healthy and arthritic mice, and classified them as mice with severe, mild, and no inflammation based on MRI and clinical findings. MSOT detected arthritic joints and distinguished different grades of arthritic inflammation. The MSOT imaging results also constituted a high correlation to MRI findings and clinical examination.

As opposed to evaluating RA through alterations to the morphology, this approach directly visualized a molecular process that represented the degree of inflammation. This allowed for accurate and objective user-independent diagnosis of arthritic inflammation even with a limited number of mice used to establish the analysis method and the evaluation of imaging results.

MSOT could also directly visualize and quantify blood and vascular structures through the accurate and specific detection of oxygenated and deoxygenated hemoglobin. As inflammation is typically accompanied by changes in the blood circulation and the composition of oxy- and deoxygenated hemoglobin, MSOT could simultaneously determine additional pathological information for the diagnosis of arthritic inflammation. Moreover, this allowed for cross-referencing of contrast agent localization and blood stream.

With further investigation and an increased number of mice in future experiments, the analysis method could be further optimized and a more detailed and accurate comparison and correlation with MR imaging and other imaging modalities could be established. However,

these results showed that it is feasible to use MSOT imaging to accurately detect arthritic inflammation using an inflammation targeting contrast agent.

Moreover, further development of the imaging technique could improve the use of MSOT for the quantification of inflammation. Currently, only one 2-dimensional slice can be scanned at the same time. However, quantification of the volume of the inflamed joint tissue would be even more accurate than determining the area in a single slice. Systems with actual 3-dimensional imaging with isotropic spatial resolution for the illumination target volume would significantly improve the precision for the assessment of arthritic inflammation (A. Taruttis et al., 2013).

5.7. Therapy Monitoring

The treatment response in mice was evaluated using MSOT imaging with dPGS-NIR as an inflammation targeting contrast agent, and compared to MR findings, and clinical findings. At 3 different timepoints after the induction of arthritis (5, 35, 42 days) the MSOT images of mice with and without treatment were evaluated and compared with MR findings and clinical scores. The treatment consisted of methotrexate and glucocorticoids. MSOT imaging findings showed high correlation with MR findings and clinical findings. In addition, the imaging findings were confirmed histopathologically. While differences between the groups could be observed in MSOT imaging, the limited number of mice used for this experiment did not translate into significant differences regarding the quantitative MSOT contrast agent signal between mice with and without therapy. At 42 days after the induction the clinical scores between mice with and without therapy showed the largest difference, while the MSOT images displayed very similar results at day 35 and day 42. These results indicate that MSOT imaging could detect an appropriate therapy response at 35 days after the induction, even before the clinical signs reveal the full effect of treatment at 42 days after the arthritis induction. This could mean that MSOT imaging might serve as a means to distinguish patients that are highly responsive to specific treatment from those that are not at an early point in time as the accumulation of dPGS reflects the responsiveness and effectiveness of the medication. Subsequently, this could allow for differentiation between responders and non-responders of a certain therapy because dPGS-NIR MSOT directly visualizes the increase of inflammatory inhibition through medication. This discrimination could be done before any changes in the symptoms of the patient would be observable, similar to current MRI dependent treatment monitoring assessment (Hodgson et al., 2008). Hereby, the treatment could be modified earlier and might improve the outcome for patients overall, and more specifically for those patients that show a weak treatment response.

The imaging results showed high variance, the main reason being significant differences in the severity of the arthritic inflammation between mice of the same group. In addition, treatment responses of the mice can vary widely. This was also represented by the high standard

deviation of the clinical scores, signifying clear differences between the mice in the development and clinical outcome of the disease.

Optoacoustic imaging has previously been used in rat model of RA arthritis to measure the development of angiogenesis in healthy and arthritic rats with and without treatment (Rajian, Shao, Chamberland, & Wang, 2013). These findings were compared to MicroPET images as a gold standard. This study also showed similar limitations regarding the high variance of the imaging results and the clinical signs based on the inhomogeneity in the development and severity of the RA model. Their imaging setup, however, was combined with traditional ultrasonography and only allowed for the depiction of one transverse plane, and only relied on the evaluation of hemodynamic characteristics of the joint. Using MSOT with inflammation targeting contrast agent in a murine model, tomographic images of the entire leg could be acquired with more detailed molecular information regarding the inflammation. Notably, dPGS could also be used in a therapeutic approach to treat RA, as it was shown to inhibit inflammation. A dPGS based contrast agent would have the intriguing property to accurately visualize the site of action in treated patients.

5.8. Comparison to Other OI and Clinical Imaging Modalities

Overall, MSOT represents a promising imaging modality that could easily be used for the detection and evaluation of human RA in a clinical setting. MSOT has already shown to be a very useful clinical imaging tool for a variety of diseases (A. Taruttis, van Dam, & Ntziachristos, 2015).

5.8.1. OI Systems

MSOT combines several the advantages of optical imaging (OI), while the limitations are very limited compared to other OI techniques. MSOT offers imaging of anatomical structures through endogenous tissue contrast with a spatial resolution of 200µm. Additionally, MSOT allows for tomographic or 3-dimensional image reconstruction, as opposed to planar optical imaging methods such as the commercially available Xiralite X4 (Mivenion, Berlin) for the detection of RA. Planar imaging limits the spatial resolution and precise evaluation of anatomical structures. Accurate and reliable assessment of the synovia and its status of inflammation was more difficult using the Xiralite X4. As this is a major sign for detection for arthritis, this ICG-enhanced optical imaging system showed limitations in the detection of synovitis compared to MRI – an imaging modality that provides reliable assessment of the synovia (Meier et al., 2012). While Xiralite X4 could accurately diagnose highly inflamed joints, it more specifically showed limitations in the diagnosis of low to mild inflammation levels. MSOT, however, was able to reliably depict the joint structures of the knee joint in mice with high spatial resolution and showed tomographic imaging results comparable to MR imaging.

Fluorescence Molecular Tomography (FMT) is an optical imaging system that also provides tomographic imaging with high spatial resolution and the possibility of 3-dimensional reconstruction. FMT is a fluorescence based optical imaging system that illuminates the object circularly through a rotating laser, similarly to x-ray illumination in a CT. In a study, indocyanine green (ICG) enhanced FMT was used to detect and characterize synovitis in joints of patients with RA and could distinguish arthritic from healthy joints. FMT allowed for depth-resolved imaging of the joints and could be used to detect synovitis in patients with RA (Mohajerani et al., 2014). Compared to FMT, MSOT additionally provided accurate visualization of oxy- and deoxygenated hemoglobin through fast multispectral imaging data acquisition, another parameter which could help characterize synovitis and further improve the diagnostic reliability. Also, MSOT does not rely on fluorescence for imaging data acquisition, but only on the light absorption properties of the specimen. This enables the use and evaluation of a much larger variety of items for optoacoustic imaging such as gold nanorods. Moreover, optical scattering within tissue is higher than scattering of ultrasound waves (Ntziachristos & Razansky, 2010). In theory, this allows for a higher penetration depth of optoacoustic imaging system, especially under future improvement of the imaging modality regarding illumination and detection techniques, as well as reconstruction algorithms.

5.8.2. Conventional Radiography

Conventional radiography can readily assess more severe damages to bone and cartilage. However, compared to MSOT, it cannot evaluate synovitis or other early and more subtle changes to the joint. That's why conventional radiography, as opposed to MSOT, is not as well suited for the early detection of RA. Rather, conventional radiography can be used to evaluate more severe changes to bone and cartilage at the later stages of the disease. Imaging of bone structures, however, is one of the key limitations of MSOT as light is heavily attenuated through bone. Moreover, conventional radiography only offers planar imaging of the joint, while MSOT allows for tomographic and 3-dimensional image reconstruction. Overall, conventional radiography is widely accessible, very fast, and inexpensive imaging modality for RA (Llopis, Kroon, Acosta, & Bloem, 2017).

5.8.3. Ultrasonography

Similarly to MSOT, Ultrasonography (US) offers high soft tissue contrast, and can visualize perfusion of the joint. This way, US can be used to detect and assess active arthritis in the joint, e.g. through the evaluation of the synovia and the cartilage. Hence, both US and MSOT are able to detect RA at the earlier stages when solely alterations to the synovia are observable, while they both show limitations regarding imaging through bone. In contrast to

MSOT imaging with a standardized imaging protocol, ultrasonography is very user-dependent, and the experience of the examiner largely determines its accuracy (Ten Cate et al., 2013). Overall, ultrasonography offers a very accessible and cheap imaging modality that is routinely used as an imaging modality to assess whether a joint is affected as recommended in the 2010 Rheumatoid Arthritis Classification Criteria (Aletaha et al., 2010).

5.8.4. MRI

MRI combines high anatomical resolution of both soft tissue and bone structures with high endogenous contrast. In addition, contrast agents can further improve tissue contrast. The evaluation of contrast agent enhancement and dynamics can identify inflamed tissue. As MRI reveals a wide range of morphological pathologies typical for RA, as well as changes in the contrast-agent dynamics that are typical for inflamed tissue, it has evolved into the gold standard of imaging for RA (McQueen, 2014).

In our experiments, we found the MR imaging results to be very much comparable to those of the MSOT, as both MR and MSOT were able to accurately visualize the degree of inflammation in the joint through visualization of the joint structures, and its contrast agent dynamics. Hereby, MSOT and MR showed similar strengths in the visualization of soft tissue. In contrast to MSOT, however, MRI can additionally identify pathological alterations to bone structures very accurately and reliably. Thus, MRI represents the most powerful clinical imaging tool in the detection of bone erosions and bone edema (McQueen, 2014). With the use of contrast agent enhanced MRI, the evaluation of contrast agent dynamics also allows for the grading of inflammatory activity in the joint. Both MRI and MSOT can accurately identify synovitis, and thus could detect RA at very early stages of the disease. Using standardized MR imaging and analysis protocols such as RAMRIS, MRI also achieves high inter-reader reliability, hence offering an objective way to grade and stage RA. Moreover, MRI easily provides imaging of large joints such as the knee, while MSOT imaging is constrained to smaller joints such as the fingers because of the rather low penetration depth of light in tissue (Ntziachristos & Razansky, 2010). However, MRI entails some disadvantages that pose a strong limitation to its widespread use: Long acquisition times, high imaging and maintenance costs, and restricted accessibility. Therefore, extensive use of MRI for detection and assessment of joints from affected patients, or even employing MRI to screen a certain population for RA is not feasible (Borrero, Mountz, & Mountz, 2011). MSOT, however, is an inexpensive, and easy to use imaging modality.

5.9. Outlook – MSOT in a Clinical Setting

MSOT represents a clinically applicable imaging modality that allows for accurate imaging of soft tissue with high resolution. It can be combined with contrast agents to further increase soft tissue contrast and evaluate contrast agent dynamics for the detection of inflammation. While fluorescent contrast agents such as ICG are also allowed for clinical use, more contrast agents are under development, particularly those with specific targeting mechanisms. In this study, we showed the potential for an inflammation targeting contrast agent in the detection and evaluation of RA, as it allowed for accurate diagnosis and grading of the inflammation of RA.
MSOT could easily be translated into clinical routine with minimal adaption of the hardware.
However, MSOT showed limitations in the imaging of and through bone. Evaluation of damages to the bone is needed to accurately assess the extent of the disease. A multimodal imaging approach combining MSOT with conventional radiography could overcome the challenge of accurate visualization of bone structures and potential damages to the bone. Multimodal imaging approaches, overall, become increasingly more popular and are already being applied for the imaging of RA. Ultrasonography, and conventional radiography are routinely used for this purpose, as the combination of the two offers assessment of the joints comprising both soft and hard tissue. In addition, MSOT could be used for the early detection of RA through accurate visualization of inflammation in the joint, and more specifically synovitis. MSOT could provide continuous and low-cost evaluation of the inflammatory degree in the joints of patients to monitor progression of the disease and the efficacy of the therapy. Using MSOT for the imaging of RA might avoid expensive MR imaging procedures and thus significantly lower medical costs.

5.10. Conclusion

MSOT using the inflammation-targeting optoacoustic contrast agent dPGS-NIR was able to accurately visualize the joint and the extent of arthritic inflammation as confirmed by MRI, clinical observation, and histopathology. A standardized MSOT image analysis protocol was successfully developed to objectively detect and grade arthritic inflammation. This way MSOT could distinguish between inflamed and healthy joints and grade the degree of the arthritic inflammation from mild to severe in an easy and mostly user-independent fashion. Furthermore, dPGS coated gold nanorods (AuNR-dPGS) were able to serve as very suitable optoacoustic contrast agents that could accurately visualize arthritic inflammation in the joints. Finally, MSOT showed potential to monitor treatment efficacy, though the results remained partly inconclusive. However, these results might be attributed to a limited number of experiments in a murine model with high variability in the development of the disease.
Overall, MSOT demonstrated to be very suitable for the imaging of RA in a murine model. It could easily be translated into clinical practice as an inexpensive, easy-to-use, and user-

independent way to assess RA in patients. The limitations of MSOT regarding imaging of bone could be overcome by combining it with other imaging systems such as conventional radiography in a multimodal imaging approach.

6. Summary

Rheumatoid arthritis (RA) is one of the most common chronic inflammatory diseases, primarily causing inflammation of the joint. To evaluate multispectral optoacoustic tomography (MSOT) for the detection and staging of RA, the extent of the inflammation in the joint was visualized in a murine model through inflammation targeting contrast agents. A collagen induced arthritis model was used as a RA model of the limb. MSOT imaging was performed with a near-infrared dye (NIR) and gold nanorods (AuNR) as contrast agents, both targeting the inflammatory surface proteins L- and P- selectin with polyanionic dendritic polyglycerol sulfate (dPGS). Contrast enhanced MR imaging as well as clinical observation, lymphocyte to granulocyte count and histopathology served as references. MSOT using a dPGS coated near-infrared dye (dPGS-NIR) as an inflammation targeting contrast agent allowed for accurate diagnosis and for significant differentiation between inflamed and healthy joints ($P = 0.023$). Additionally, we investigated whether MSOT could be suitable to monitor the efficacy of treatment for RA. Differences between the group that received therapy to the group that did not receive treatment were observed. However, the differences were not significant presumably because of limited number of experiments and high variability of the arthritis model. Furthermore, dPGS coated gold nanorods (AuNR-dPGS) were also able to accurately visualize arthritic inflammation in the joints. In conclusion, MSOT using an inflammation targeting photoacoustic contrast agent was a reliable and accurate imaging method to assess RA. This approach could easily be translated into clinical practice as an inexpensive, easy-to-use, and user-independent imaging modality for the assessment of RA.

7. Appendix

7.1. References

Aletaha, D., Neogi, T., Silman, A. J., Funovits, J., Felson, D. T., Bingham, C. O., 3rd, . . . Hawker, G. (2010). 2010 Rheumatoid arthritis classification criteria: an American College of Rheumatology/European League Against Rheumatism collaborative initiative. *Arthritis Rheum, 62*(9), 2569-2581. doi:10.1002/art.27584

Andersson, S. E., Lexmuller, K., & Ekstrom, G. M. (1998). Physiological characterization of mBSA antigen induced arthritis in the rat. I. Vascular leakiness and pannus growth. *J Rheumatol, 25*(9), 1772-1777.

Biffi, S., Dal Monego, S., Dullin, C., Garrovo, C., Bosnjak, B., Licha, K., . . . Alves, F. (2013). Dendritic polyglycerolsulfate near infrared fluorescent (NIRF) dye conjugate for non-invasively monitoring of inflammation in an allergic asthma mouse model. *PLoS One, 8*(2), e57150. doi:10.1371/journal.pone.0057150

Boreham, A., Pikkemaat, J., Volz, P., Brodwolf, R., Kuehne, C., Licha, K., . . . Alexiev, U. (2015). Detecting and Quantifying Biomolecular Interactions of a Dendritic Polyglycerol Sulfate Nanoparticle Using Fluorescence Lifetime Measurements. *Molecules, 21*(1), E22. doi:10.3390/molecules21010022

Borrero, C. G., Mountz, J. M., & Mountz, J. D. (2011). Emerging MRI methods in rheumatoid arthritis. *Nat Rev Rheumatol, 7*(2), 85-95. doi:10.1038/nrrheum.2010.173

Brand, D. D., Latham, K. A., & Rosloniec, E. F. (2007). Collagen-induced arthritis. *Nat Protoc, 2*(5), 1269-1275. doi:10.1038/nprot.2007.173

Buehler, A., Rosenthal, A., Jetzfellner, T., Dima, A., Razansky, D., & Ntziachristos, V. (2011). Model-based optoacoustic inversions with incomplete projection data. *Med Phys, 38*(3), 1694-1704. doi:10.1118/1.3556916

Buer, J. K. (2015). A history of the term “DMARD”. *Inflammopharmacology, 23*(4), 163-171. doi:10.1007/s10787-015-0232-5

Bugatti, S., Manzo, A., Caporali, R., & Montecucco, C. (2012). Inflammatory lesions in the bone marrow of rheumatoid arthritis patients: a morphological perspective. *Arthritis Res Ther, 14*(6), 229. doi:10.1186/ar4115

Caplazi, P., Baca, M., Barck, K., Carano, R. A., DeVoss, J., Lee, W. P., . . . Diehl, L. (2015). Mouse Models of Rheumatoid Arthritis. *Vet Pathol, 52*(5), 819-826. doi:10.1177/0300985815588612

Chen, Y. F., Jobanputra, P., Barton, P., Bryan, S., Fry-Smith, A., Harris, G., & Taylor, R. S. (2008). Cyclooxygenase-2 selective non-steroidal anti-inflammatory drugs (etodolac, meloxicam, celecoxib, rofecoxib, etoricoxib, valdecoxib and lumiracoxib) for osteoarthritis and rheumatoid arthritis: a systematic review and economic evaluation. *Health Technol Assess, 12*(11), 1-278, iii.

Cuchacovich, M., Couret, M., Peray, P., Gatica, H., & Sany, J. (1992). Precision of the Larsen and the Sharp methods of assessing radiologic change in patients with rheumatoid arthritis. *Arthritis Rheum, 35*(7), 736-739.

Cush, J. J., Weinblatt, M. E. und A. Kavanaugh, A. (2010). Rheumatoid Arthritis:

Overview, Etiology, Pathology. In *Rheumatoid Arthritis: Early Diagnosis and Treatment* (3. ed., pp. 17). West Islip: Professional Communications, Inc.

Dekkers, J. S., Schoones, J. W., Huizinga, T. W., Toes, R. E., & van der Helm-van Mil, A. H. (2017). Possibilities for preventive treatment in rheumatoid arthritis? Lessons from experimental animal models of arthritis: a systematic literature review and meta-analysis. *Annals of the Rheumatic Diseases, 76*(2), 458-467. doi:10.1136/annrheumdis-2016-209830

Dernedde, J., Rausch, A., Weinhart, M., Enders, S., Tauber, R., Licha, K., . . . Haag, R. (2010). Dendritic polyglycerol sulfates as multivalent inhibitors of inflammation. *Proc Natl Acad Sci U S A, 107*(46), 19679-19684. doi:10.1073/pnas.1003103107

Donahue, K. E., Gartlehner, G., Jonas, D. E., Lux, L. J., Thieda, P., Jonas, B. L., . . . Lohr, K. N. (2008). Systematic review: comparative effectiveness and harms of disease-modifying medications for rheumatoid arthritis. *Ann Intern Med, 148*(2), 124-134.

Farheen, K., & Agarwal, S. K. (2011). Assessment of disease activity and treatment outcomes in rheumatoid arthritis. *J Manag Care Pharm, 17*(9 Suppl B), S09-13.

Feldmann, M., Brennan, F. M., & Maini, R. N. (1996). Rheumatoid arthritis. *Cell, 85*(3), 307-310.

Finckh, A. (2009). Early inflammatory arthritis versus rheumatoid arthritis. *Curr Opin Rheumatol, 21*(2), 118-123. doi:10.1097/BOR.0b013e3283235ac4

Finckh, A., Liang, M. H., van Herckenrode, C. M., & de Pablo, P. (2006). Long-term impact of early treatment on radiographic progression in rheumatoid arthritis: A meta-analysis. *Arthritis Rheum, 55*(6), 864-872. doi:10.1002/art.22353

Fournelle, M., Bost, W., Tarner, I. H., Lehmberg, T., Weiss, E., Lemor, R., & Dinser, R. (2012). Antitumor necrosis factor-alpha antibody-coupled gold nanorods as nanoprobes for molecular optoacoustic imaging in arthritis. *Nanomedicine, 8*(3), 346-354. doi:10.1016/j.nano.2011.06.020

Furuzawa-Carballeda, J., Macip-Rodriguez, P. M., & Cabral, A. R. (2008). Osteoarthritis and rheumatoid arthritis pannus have similar qualitative metabolic characteristics and pro-inflammatory cytokine response. *Clin Exp Rheumatol, 26*(4), 554-560.

Gaffen, S. L. (2009). Role of IL-17 in the Pathogenesis of Rheumatoid Arthritis. *Current rheumatology reports, 11*(5), 365-370.

Gandjbakhch, F., Haavardsholm, E. A., Conaghan, P. G., Ejbjerg, B., Foltz, V., Brown, A. K., . . . Ostergaard, M. (2014). Determining a magnetic resonance imaging inflammatory activity acceptable state without subsequent radiographic progression in rheumatoid arthritis: results from a followup MRI study of 254 patients in clinical remission or low disease activity. *J Rheumatol, 41*(2), 398-406. doi:10.3899/jrheum.131088

Golovko, D., Meier, R., Rummeny, E., & Daldrup-Link, H. (2011). Optical imaging of rheumatoid arthritis. *Int J Clin Rheumtol, 6*(1), 67-75. doi:10.2217/ijr.10.105

Guerrero, A. R., Hassan, N., Escobar, C. A., Albericio, F., Kogan, M. J., & Araya, E. (2014). Gold nanoparticles for photothermally controlled drug release. *Nanomedicine (Lond), 9*(13), 2023-2039. doi:10.2217/nnm.14.126

Haavardsholm, E. A., Ostergaard, M., Ejbjerg, B. J., Kvan, N. P., Uhlig, T. A., Lilleas, F. G., & Kvien, T. K. (2005). Reliability and sensitivity to change of the OMERACT rheumatoid arthritis magnetic resonance imaging score in a multireader, longitudinal setting. *Arthritis Rheum, 52*(12), 3860-3867. doi:10.1002/art.21493

Herzog, E., Taruttis, A., Beziere, N., Lutich, A. A., Razansky, D., & Ntziachristos, V. (2012). Optical imaging of cancer heterogeneity with multispectral optoacoustic tomography. *Radiology, 263*(2), 461-468. doi:10.1148/radiol.11111646

Hodgson, R. J., O'Connor, P., & Moots, R. (2008). MRI of rheumatoid arthritis image quantitation for the assessment of disease activity, progression and response to therapy. *Rheumatology (Oxford), 47*(1), 13-21. doi:10.1093/rheumatology/kem250

Holmdahl, R., Jansson, L., Larsson, E., Rubin, K., & Klareskog, L. (1986). Homologous type II collagen induces chronic and progressive arthritis in mice. *Arthritis Rheum, 29*(1), 106-113.

Ibarra, J. M., Jimenez, F., Martinez, H. G., Clark, K., & Ahuja, S. S. (2011). MMP-Activated Fluorescence Imaging Detects Early Joint Inflammation in Collagen-Antibody-Induced Arthritis in CC-Chemokine Receptor-2-Null Mice, In-Vivo. *Int J Inflam, 2011*, 691587. doi:10.4061/2011/691587

Ideguchi, H., Ohno, S., Hattori, H., Senuma, A., & Ishigatsubo, Y. (2006). Bone erosions in rheumatoid arthritis can be repaired through reduction in disease activity with conventional disease-modifying antirheumatic drugs. *Arthritis Res Ther, 8*(3), R76. doi:10.1186/ar1943

Jordan, K., Clarke, A. M., Symmons, D. P. M., Fleming, D., Porcheret, M., Kadam, U. T., & Croft, P. (2007). Measuring disease prevalence: a comparison of musculoskeletal disease using four general practice consultation databases. *The British Journal of General Practice, 57*(534), 7-14.

Kamala, T. (2007). Hock immunization: a humane alternative to mouse footpad injections. *J Immunol Methods, 328*(1-2), 204-214. doi:10.1016/j.jim.2007.08.004

Khachigian, L. M. (2006). Collagen antibody-induced arthritis. *Nat Protoc, 1*(5), 2512-2516. doi:10.1038/nprot.2006.393

Ley, K., Laudanna, C., Cybulsky, M. I., & Nourshargh, S. (2007). Getting to the site of inflammation: the leukocyte adhesion cascade updated. *Nat Rev Immunol, 7*(9), 678-689. doi:10.1038/nri2156

Licha, K., Welker, P., Weinhart, M., Wegner, N., Kern, S., Reichert, S., . . . Schirner, M. (2011). Fluorescence imaging with multifunctional polyglycerol sulfates: novel polymeric near-IR probes targeting inflammation. *Bioconjug Chem, 22*(12), 2453-2460. doi:10.1021/bc2002727

Llopis, E., Kroon, H. M., Acosta, J., & Bloem, J. L. (2017). Conventional Radiology in Rheumatoid Arthritis. *Radiol Clin North Am, 55*(5), 917-941. doi:10.1016/j.rcl.2017.04.002

Ma, R., Taruttis, A., Ntziachristos, V., & Razansky, D. (2009). Multispectral optoacoustic tomography (MSOT) scanner for whole-body small animal imaging. *Opt Express, 17*(24), 21414-21426. doi:10.1364/oe.17.021414

Mallidi, S., Larson, T., Tam, J., Joshi, P. P., Karpiouk, A., Sokolov, K., & Emelianov, S. (2009). Multiwavelength photoacoustic imaging and plasmon resonance coupling of gold nanoparticles for selective detection of cancer. *Nano Lett, 9*(8), 2825-2831. doi:10.1021/nl802929u

McQueen, F. M. (2014). MRI in rheumatoid arthritis: a useful tool for the clinician? *Postgrad Med J, 90*(1064), 332-339. doi:10.1136/postgradmedj-2013-132121

McQueen, F. M., Stewart, N., Crabbe, J., Robinson, E., Yeoman, S., Tan, P. L., & McLean, L. (1998). Magnetic resonance imaging of the wrist in early rheumatoid arthritis reveals a high prevalence of erosions at four months after symptom onset. *Ann Rheum Dis, 57*(6), 350-356.

McRobbie, D. W., Moore, E. A., Graves, M. J., & Prince, M. R. (2017). *MRI from Picture to Proton* (3 ed.). Cambridge: Cambridge University Press.

Meier, R., Krug, C., Golovko, D., Boddington, S., Piontek, G., Rudelius, M., . . . Daldrup-Link, H. E. (2010). Indocyanine green-enhanced imaging of antigen-induced arthritis with an integrated optical imaging/radiography system. *Arthritis Rheum, 62*(8), 2322-2327. doi:10.1002/art.27542

Meier, R., Thurmel, K., Moog, P., Noel, P. B., Ahari, C., Sievert, M., . . . Rummeny, E. J. (2012). Detection of synovitis in the hands of patients with rheumatologic disorders: diagnostic performance of optical imaging in comparison with magnetic resonance imaging. *Arthritis Rheum, 64*(8), 2489-2498. doi:10.1002/art.34467

Mohajerani, P., Koch, M., Thurmel, K., Haller, B., Rummeny, E. J., Ntziachristos, V., & Meier, R. (2014). Fluorescence-aided tomographic imaging of synovitis in the human finger. *Radiology, 272*(3), 865-874. doi:10.1148/radiol.14132128

Muller-Ladner, U., Kriegsmann, J., Franklin, B. N., Matsumoto, S., Geiler, T., Gay, R. E., & Gay, S. (1996). Synovial fibroblasts of patients with rheumatoid arthritis attach to and invade normal human cartilage when engrafted into SCID mice. *Am J Pathol, 149*(5), 1607-1615.

Muller, J., Wunder, A., & Licha, K. (2013). Optical imaging. *Recent Results Cancer Res, 187*, 221-246. doi:10.1007/978-3-642-10853-2_7

Murphy, C. J., Sau, T. K., Gole, A. M., Orendorff, C. J., Gao, J., Gou, L., . . . Li, T. (2005). Anisotropic metal nanoparticles: Synthesis, assembly, and optical applications. *J Phys Chem B, 109*(29), 13857-13870. doi:10.1021/jp0516846

Nandakumar, K. S., & Holmdahl, R. (2007). Collagen Antibody Induced Arthritis. In A. P. Cope (Ed.), *Arthritis Research: Methods and Protocols Volume 2* (pp. 215-223). Totowa, NJ: Humana Press.

Ntziachristos, V. (2010). Going deeper than microscopy: the optical imaging frontier in biology. *Nat Methods, 7*(8), 603-614. doi:10.1038/nmeth.1483

Ntziachristos, V., & Razansky, D. (2010). Molecular imaging by means of multispectral optoacoustic tomography (MSOT). *Chem Rev, 110*(5), 2783-2794. doi:10.1021/cr9002566

Ortendahl, M., Schettler, J. D., & Fries, J. F. (2000). Factors influencing length of time taking methotrexate in rheumatoid arthritis. *J Rheumatol, 27*(5), 1139-1147.

Østergaard, M., Edmonds, J., McQueen, F., Peterfy, C., Lassere, M., Ejbjerg, B., . . . Conaghan, P. (2005). An introduction to the EULAR–OMERACT rheumatoid arthritis MRI reference image atlas. *Annals of the Rheumatic Diseases, 64*(suppl 1), i3-i7. doi:10.1136/ard.2004.031773

Ostergaard, M., Ejbjerg, B., & Szkudlarek, M. (2005). Imaging in early rheumatoid arthritis: roles of magnetic resonance imaging, ultrasonography, conventional radiography and computed tomography. *Best Pract Res Clin Rheumatol, 19*(1), 91-116. doi:10.1016/j.berh.2004.08.006

Ostergaard, M., Klarlund, M., Lassere, M., Conaghan, P., Peterfy, C., McQueen, F., . . . Edmonds, J. (2001). Interreader agreement in the assessment of magnetic resonance images of rheumatoid arthritis wrist and finger joints--an international multicenter study. *J Rheumatol, 28*(5), 1143-1150.

Ostergaard, M., Peterfy, C., Conaghan, P., McQueen, F., Bird, P., Ejbjerg, B., . . . Edmonds, J. (2003). OMERACT Rheumatoid Arthritis Magnetic Resonance Imaging Studies. Core set of MRI acquisitions, joint pathology definitions, and the OMERACT RA-MRI scoring system. *J Rheumatol, 30*(6), 1385-1386.

Pichler, B. J., Wehrl, H. F., & Judenhofer, M. S. (2008). Latest advances in molecular imaging instrumentation. *J Nucl Med, 49 Suppl 2*, 5s-23s. doi:10.2967/jnumed.108.045880

Puszczewicz, M., & Iwaszkiewicz, C. (2011). Role of anti-citrullinated protein antibodies in diagnosis and prognosis of rheumatoid arthritis. *Arch Med Sci, 7*(2), 189-194. doi:10.5114/aoms.2011.22067

Put, S., Westhovens, R., Lahoutte, T., & Matthys, P. (2014). Molecular imaging of rheumatoid arthritis: emerging markers, tools, and techniques. *Arthritis Res Ther, 16*(2), 208. doi:10.1186/ar4542

Qin, H., Zhao, Y., Zhang, J., Pan, X., Yang, S., & Xing, D. (2016). Inflammation-targeted gold nanorods for intravascular photoacoustic imaging detection of matrix metalloproteinase-2 (MMP2) in atherosclerotic plaques. *Nanomedicine, 12*(7), 1765-1774. doi:10.1016/j.nano.2016.02.016

Rajian, J. R., Shao, X., Chamberland, D. L., & Wang, X. (2013). Characterization and treatment monitoring of inflammatory arthritis by photoacoustic imaging: a study on adjuvant-induced arthritis rat model. *Biomed Opt Express, 4*(6), 900-908. doi:10.1364/boe.4.000900

Ravindran, V., Rachapalli, S., & Choy, E. H. (2009). Safety of medium- to long-term glucocorticoid therapy in rheumatoid arthritis: a meta-analysis. *Rheumatology (Oxford), 48*(7), 807-811. doi:10.1093/rheumatology/kep096

Rayavarapu, R. G., Petersen, W., Hartsuiker, L., Chin, P., Janssen, H., van Leeuwen, F. W., . . . van Leeuwen, T. G. (2010). In vitro toxicity studies of polymer-coated gold nanorods. *Nanotechnology, 21*(14), 145101. doi:10.1088/0957-4484/21/14/145101

Raymond, K. N., & Pierre, V. C. (2005). Next generation, high relaxivity gadolinium MRI agents. *Bioconjug Chem, 16*(1), 3-8. doi:10.1021/bc049817y

Razansky, D., Buehler, A., & Ntziachristos, V. (2011). Volumetric real-time multispectral optoacoustic tomography of biomarkers. *Nat Protoc, 6*(8), 1121-1129. doi:10.1038/nprot.2011.351

Rosenthal, A., Razansky, D., & Ntziachristos, V. (2010). Fast semi-analytical model-based acoustic inversion for quantitative optoacoustic tomography. *IEEE Trans Med Imaging, 29*(6), 1275-1285. doi:10.1109/TMI.2010.2044584

Scheel, A. K., Backhaus, M., Klose, A. D., Moa-Anderson, B., Netz, U. J., Hermann, K. G., . . . Hielscher, A. H. (2005). First clinical evaluation of sagittal laser optical tomography for detection of synovitis in arthritic finger joints. *Ann Rheum Dis, 64*(2), 239-245. doi:10.1136/ard.2004.024224

Schurgers, E., Billiau, A., & Matthys, P. (2011). Collagen-induced arthritis as an animal model for rheumatoid arthritis: focus on interferon-gamma. *J Interferon Cytokine Res, 31*(12), 917-926. doi:10.1089/jir.2011.0056

Sievert, M. (2015). *Therapiekontrolle von inflammatorischen Arthritiden der Finger- und Handgelenke mittels quantitativer Perfusionsanalyse von fluoreszenz-optischer Bildgebung und kontrastverstärkter Magnetresonanztomographie.* Technische Universität München, Munich, Germany.

Singh, J. A., Christensen, R., Wells, G. A., Suarez-Almazor, M. E., Buchbinder, R., Lopez-Olivo, M. A., . . . Tugwell, P. (2009). Biologics for rheumatoid arthritis: an overview of Cochrane reviews. *Cochrane Database Syst Rev*(4), Cd007848. doi:10.1002/14651858.CD007848.pub2

Singh, J. A., Saag, K. G., Bridges, S. L., Jr., Akl, E. A., Bannuru, R. R., Sullivan, M. C., . . . McAlindon, T. (2016). 2015 American College of Rheumatology Guideline for the Treatment of Rheumatoid Arthritis. *Arthritis Rheumatol, 68*(1), 1-26. doi:10.1002/art.39480

Smolen, J. S., Aletaha, D., & McInnes, I. B. (2016). Rheumatoid arthritis. *Lancet, 388*(10055), 2023-2038. doi:10.1016/S0140-6736(16)30173-8

Sommer, O. J., Kladosek, A., Weiler, V., Czembirek, H., Boeck, M., & Stiskal, M. (2005). Rheumatoid Arthritis: A Practical Guide to State-of-the-Art Imaging, Image Interpretation, and Clinical Implications. *RadioGraphics, 25*(2), 381-398. doi:10.1148/rg.252045111

Stone, J., Jackson, S., & Wright, D. (2011). Biological applications of gold nanorods. *Wiley Interdiscip Rev Nanomed Nanobiotechnol, 3*(1), 100-109. doi:10.1002/wnan.120

Tan, Y. K., Ostergaard, M., & Conaghan, P. G. (2012). Imaging tools in rheumatoid arthritis: ultrasound vs magnetic resonance imaging. *Rheumatology (Oxford), 51 Suppl 7*, vii36-42. doi:10.1093/rheumatology/kes329

Taruttis, A., & Ntziachristos, V. (2012). Translational Optical Imaging. *American Journal of Roentgenology, 199*(2), 263-271. doi:10.2214/AJR.11.8431

Taruttis, A., van Dam, G. M., & Ntziachristos, V. (2015). Mesoscopic and macroscopic optoacoustic imaging of cancer. *Cancer Res, 75*(8), 1548-1559. doi:10.1158/0008-5472.Can-14-2522

Taruttis, A., Wildgruber, M., Kosanke, K., Beziere, N., Licha, K., Haag, R., . . . Ntziachristos, V. (2013). Multispectral optoacoustic tomography of myocardial infarction. *Photoacoustics, 1*(1), 3-8. doi:10.1016/j.pacs.2012.11.001

Ten Cate, D. F., Luime, J. J., Swen, N., Gerards, A. H., De Jager, M. H., Basoski, N. M., . . . Jacobs, J. W. (2013). Role of ultrasonography in diagnosing early rheumatoid arthritis and remission of rheumatoid arthritis--a systematic review of the literature. *Arthritis Res Ther, 15*(1), R4. doi:10.1186/ar4132

van der Helm-van Mil, A. H., Detert, J., le Cessie, S., Filer, A., Bastian, H., Burmester, G. R., . . . Raza, K. (2008). Validation of a prediction rule for disease outcome in patients with recent-onset undifferentiated arthritis: moving toward individualized treatment decision-making. *Arthritis Rheum, 58*(8), 2241-2247. doi:10.1002/art.23681

van der Helm-van Mil, A. H., & Huizinga, T. W. (2012). The 2010 ACR/EULAR criteria for rheumatoid arthritis: do they affect the classification or diagnosis of rheumatoid arthritis? *Ann Rheum Dis, 71*(10), 1596-1598. doi:10.1136/annrheumdis-2012-201426

van der Helm-van Mil, A. H., Verpoort, K. N., Breedveld, F. C., Toes, R. E., & Huizinga, T. W. (2005). Antibodies to citrullinated proteins and differences in clinical progression of rheumatoid arthritis. *Arthritis Res Ther, 7*(5), R949-958. doi:10.1186/ar1767

Vonnemann, J., Beziere, N., Bottcher, C., Riese, S. B., Kuehne, C., Dernedde, J., . . . Haag, R. (2014). Polyglycerolsulfate functionalized gold nanorods as optoacoustic signal nanoamplifiers for in vivo bioimaging of rheumatoid arthritis. *Theranostics, 4*(6), 629-641. doi:10.7150/thno.8518

Wang, M. Y., Wang, X. B., Sun, X. H., Liu, F. L., & Huang, S. C. (2016). Diagnostic value of high-frequency ultrasound and magnetic resonance imaging in early rheumatoid arthritis. *Exp Ther Med, 12*(5), 3035-3040. doi:10.3892/etm.2016.3695

Wang, X., Xie, X., Ku, G., Wang, L. V., & Stoica, G. (2006). Noninvasive imaging of hemoglobin concentration and oxygenation in the rat brain using high-resolution photoacoustic tomography. *J Biomed Opt, 11*(2), 024015. doi:10.1117/1.2192804

Wienecke, T., & Gotzsche, P. C. (2004). Paracetamol versus nonsteroidal anti-inflammatory drugs for rheumatoid arthritis. *Cochrane Database Syst Rev*(1), Cd003789. doi:10.1002/14651858.CD003789.pub2

Wunder, A., Straub, R. H., Gay, S., Funk, J., & Muller-Ladner, U. (2005). Molecular imaging: novel tools in visualizing rheumatoid arthritis. *Rheumatology (Oxford), 44*(11), 1341-1349. doi:10.1093/rheumatology/keh709

Yu, C., & Irudayaraj, J. (2007). Multiplex biosensor using gold nanorods. *Anal Chem, 79*(2), 572-579. doi:10.1021/ac061730d

Zeiderman, M. R., Morgan, D. E., Christein, J. D., Grizzle, W. E., McMasters, K. M., & McNally, L. R. (2016). Acidic pH-targeted chitosan capped mesoporous silica coated gold nanorods facilitate detection of pancreatic tumors via multispectral optoacoustic tomography. *ACS Biomater Sci Eng, 2*(7), 1108-1120. doi:10.1021/acsbiomaterials.6b00111

Zeman, M. N., & Scott, P. J. (2012). Current imaging strategies in rheumatoid arthritis. *Am J Nucl Med Mol Imaging, 2*(2), 174-220.

7.2. List of figures

7.3. List of tables

7.4. Eidesstattliche Erklärung

Hiermit versichere ich, Claudio Freiherr von Schacky auf Schönfeld, dass ich meine Doktorarbeit „Multispectral Optoacoustic Imaging of Rheumatoid Arthritis“ selbstständig und ohne fremde Hilfe angefertigt habe und dass ich alle von anderen Autoren wörtlich übernommenen Stellen wie auch die sich an die Gedankengänge anderer Autoren enganlegenden Ausführungen meiner Arbeit besonders gekennzeichnet und die Quellen zitiert habe. Die bildgebenden Untersuchungen dieser Studie und deren Auswertung wurden von mir eigenständig durchgeführt.

München, den

Claudio von Schacky

7.5. Acknowledgements

Firstly, I want to thank Prof. Dr. Reinhard Meier and Prof. Dr. Ernst Rummeny of the Department of Diagnostic and Interventional Radiology, rechts der Isar hospital, university hospital of the Technische Universität München, for the possibility to conduct this fantastic research and their generous help throughout the whole research project.

Secondly, I want to thank Dr. Yvonne Kosanke for her extensive help with the experiments and the animal care, and Dr. Melanie Kim for her help with the laboratory experiments as part of the molecular imaging laboratory of the rechts der Isar hospital.

In particular, I want to thank Dr. Nicolas de Beziere, Dr. Antonio Nunes, and Prof. Dr. Vasilis Ntziachristos for the very productive and fruitful collaboration to conduct these exciting experiments with the HelmholtzZentrum München, Institute of Biological and Medical Imaging.

For the very productive collaboration regarding the histopathological analysis I want to thank Dr. Michaela Aichler and Prof. Dr. med. Axel Karl Walch with the Research Unit Analytical Pathology, HelmholtzZentrum münchen.

Additionally, I want to thank Dr. Kai Licha for his collaboration on the dPGS-NIR contrast agent.

Moreover, I want to thank Dr. Jonathan Vonnemann and Prof. Dr. Rainer Haag from the Institute of Chemistry and Biochemistry of the Freie Universität Berlin for the collaboration on the exciting imaging experiments with gold nanorods.

Finally, I want to thank my family for their great support throughout the whole research project.

7.6. Publications

Beziere, N., **von Schacky, C.**, Kosanke, Y., Kimm, M., Nunes, A., Licha, K., Aichler M., Walch A., Rummeny EJ., Ntziachristos V., Meier, R. (2014). Optoacoustic imaging and staging of inflammation in a murine model of arthritis. Arthritis Rheumatol, 2014 Aug; 66(8), 2071-2078. doi:10.1002/art.38642

Vonnemann, J., Beziere, N., Bottcher, C., Riese, S. B., Kuehne, C., Dernedde, J., Licha K., **von Schacky, C**, Kosanke, Y., Kimm, K., Meier, R, Ntziachristos, V., Haag, R.: Polyglycerolsulfate functionalized gold nanorods as optoacoustic signal nanoamplifiers for in vivo bioimaging of rheumatoid arthritis. Theranostics, 2014 Mar; 4(6), 629-641.; doi:10.7150/thno.8518